Spatial radiative feedbacks from internal variability using multiple regression

Article

Supplemental Material

www.reading.ac.uk/centaur

CentAUR

Central Archive at the University of Reading

Supplemental Material for "Spatial radiative feedbacks from internal variability using multiple regression"

Jonah Bloch-Johnson, Maria A. A. Rugenstein, and Dorian S. Abbot

January 31, 2020

Contents

1 Tables

1.1 Simulations

This paper uses simulations from the LongRunMIP archive (Rugenstein et al., 2019). Specifically, we used the six models with thousand-plus year long control simulations with monthly data available at the time of this study. These models and simulations are summarized in this table:

Table S1: Atmosphere-ocean general circulation model simulations used in this study, from the LongRunMIP archive (Rugenstein et al., 2019). We use the first 1000 years of all abrupt4x simulations.

| model abbreviation | resolution | | simulation years | reference |
	atmosphere	ocean	control	
CESM104	96×144	384×320	1000	Rugenstein et al. (2016)
CNRMCM61	128×256	294×362	2000	Voldoire et al. (2019)
GISSE2R	90×144	180×288	5225	Nazarenko et al. (2015); Rind et al. (2018)
HadCM3L	73×96	73×96	1000	Cao et al. (2016)
IPSLCM5A	96×96	149×182	1000	Dufresne et al. (2013)
MPISEM12	96×192	220×256	1237	Mauritsen et al. (2019)

1.2 Error tables

1.2.1 Averaging

In the Appendix of the main text, we discuss four options for averaging the control time series when estimating feedbacks:

- *seasonal*, in which the time series is averaged into seasonal values and then four separate regressions are performed to estimate a feedback for each season,

- *monthly*, in which the time series is averaged into monthly values and then twelve separate regressions are performed to estimate a feedback for each month,

- *annual*, in which the time series is averaged into annual values and then just one regression is performed to estimate a single feedback

- *all months*, in which the time series is kept as monthly values and then just one regression is performed across all months to estimate a single feedback

We can assess their relative skill by evaluating the error metrics from Tables 1 and 2 in the main text for the net feedback.

Table S2: Like Table 1 in the main body of the text, but for the different averaging approaches discussed above, and for the net feedback. There are not significant differences in skill between the different approaches.

| | seasonal | | | annual | | | all months | | | monthly | | |
	MR	global	local	MR	global	local	MR	global	local	MR	global	local
early	0.69	0.74	2.54	0.69	0.63	2.47	0.72	0.78	2.58	0.84	0.76	2.54
late	0.29	0.26	1.87	0.33	0.35	1.81	0.31	0.27	1.85	0.47	0.23	1.84
change	0.44	0.73	0.78	0.45	0.73	0.74	0.44	0.73	0.87	0.46	0.73	0.85

Table S3: Like Table S2, but for spatial errors. Once more, there is not a significant difference between approaches.

| | seasonal | | | annual | | | all months | | | monthly | | |
	MR	global	local	MR	global	local	MR	global	local	MR	global	local
early	1.02	3.41	2.77	0.93	3.58	2.68	1.23	3.04	2.86	1.46	3.05	2.87
late	0.8	3.08	1.86	0.69	3.17	1.82	0.96	2.71	1.88	1.2	2.74	1.86
change	0.74	1.14	1.26	0.72	1.19	1.23	0.83	1.11	1.36	0.86	1.13	1.37

1.2.2 Individual models

Table S4: Errors in the normalized spatial pattern of net TOA flux change (like Table 2 in the text), but calculated for individual models. In all cases, the MR method outperforms the others in estimating the response.

| | CESM104 | | | CNRMCM61 | | | GISSE2R | | | HadCM3L | | | IPSLCM5A | | | MPIESM12 | | |
	MR	glob	local	MR	glob	local	MR	glob	local	MR	glob	local	MR	glob	local	MR	glob	local
early	1.68	6.86	3.36	1.10	1.36	1.61	2.57	4.10	3.54	1.95	5.88	3.79	1.38	4.45	3.72	1.72	5.56	4.29
late	1.38	7.61	2.52	1.24	1.45	1.48	0.93	2.79	1.66	1.88	4.88	2.95	1.52	4.70	3.05	1.47	5.14	2.95
change	1.45	1.93	1.71	1.06	1.18	1.25	2.49	2.93	3.20	1.87	2.64	2.16	1.03	1.42	1.30	1.50	1.92	2.08

1.2.3 North of 30°S

Figure 7 in the text suggests that the MR method is able to recreate the multi-model mean behavior of $\vec{N}$ north of 30°S. We test this idea by reevaluating the error metrics in Table 1 and 2 using only TOA fluxes from this region.

Table S5: Like Table 1 in the text, but only using TOA fluxes from north of 30°S.

| | net | | | LW clear | | | SW clear | | | LW cloud | | | SW cloud | | |
	MR	global	local	MR	global	local	MR	global	local	MR	global	local	MR	global	local
early	0.48	0.86	2.86	0.13	0.26	0.71	0.08	0.17	0.06	0.16	0.42	1.4	0.38	0.76	1.35
late	0.23	0.4	2.03	0.22	0.65	0.5	0.08	0.25	0.08	0.11	0.5	1.14	0.21	0.45	0.88
change	0.38	0.87	0.89	0.1	0.5	0.28	0.08	0.14	0.08	0.1	0.12	0.32	0.24	0.55	0.51

Table S6: Like Table 2 in the text, but only using TOA fluxes from north of 30°S.

| | net | | | LW clear | | | SW clear | | | LW cloud | | | SW cloud | | |
	MR	global	local	MR	global	local	MR	global	local	MR	global	local	MR	global	local
early	0.8	3.78	3.02	0.35	2.35	1.13	0.83	0.98	0.74	0.75	5.88	2.41	1.11	5.65	2.54
late	0.6	3.46	1.95	0.38	2.39	0.83	0.79	1.03	0.73	0.54	5.8	1.8	0.96	5.53	1.85
change	0.67	1.18	1.27	0.28	0.79	0.47	0.45	0.74	0.44	0.6	0.79	0.92	0.81	1.27	1.21

1.3 Feedbacks for individual models

Table S7: True feedback values and estimates of these values using the global and local methods for all models and flux components. All feedbacks have units of $Wm^{-2}K^{-1}$.

| | | *true* | | | | | *global* | | | | | *local* | | | |
| | | LW | SW | LW | SW | | LW | SW | LW | SW | | LW | SW | LW | SW |
model	net	clear	clear	cloud	cloud	net	clear	clear	cloud	cloud	net	clear	clear	cloud	cloud
early															
CESM104	-1.48	-1.92	0.92	0.04	-0.51	-1.13	-2.08	0.64	0.21	0.11	1.23	-1.08	0.92	2.2	-0.81
CNRMCM61	-0.89	-1.8	0.85	0.29	-0.23	-0.47	-1.86	1.3	0.36	-0.29	0.33	-1.6	0.86	0.33	0.74
GISSE2R	-2.52	-1.84	0.4	0.21	-1.29	-1.05	-1.8	0.55	0.49	-0.29	-0.95	-1.24	0.36	0.81	-0.88
HadCM3L	-1.51	-1.94	0.43	0.52	-0.53	-0.93	-1.84	0.45	0.9	-0.44	1.46	-1.3	0.45	0.9	1.41
IPSLCM5A	-0.88	-2.02	0.55	0.07	0.53	-0.37	-1.81	0.64	0.93	-0.14	1.87	-1.27	0.52	1.71	0.91
MPIESM12	-1.71	-1.84	0.61	0.4	-0.88	-1.2	-1.89	0.59	0.99	-0.89	1.61	-1.27	0.6	1.33	0.94
mean	-1.5	-1.89	0.63	0.25	-0.49	-0.86	-1.88	0.7	0.65	-0.32	0.92	-1.29	0.62	1.21	0.38
mean (no GISSE2R)	-1.29	-1.9	0.67	0.26	-0.32	-0.82	-1.9	0.73	0.68	-0.33	1.3	-1.3	0.67	1.29	0.64
late															
CESM104	-0.78	-1.84	1.05	0.1	-0.09	-1.15	-2.09	0.65	0.21	0.09	1.23	-1.19	1.19	1.91	-0.69
CNRMCM61	-0.59	-1.63	0.6	0.27	0.19	-0.47	-1.86	1.31	0.36	-0.28	0.35	-1.56	0.93	0.39	0.58
GISSE2R	-1.29	-1.53	0.42	0.36	-0.54	-1.03	-1.8	0.56	0.47	-0.26	-0.78	-1.32	0.42	0.82	-0.7
HadCM3L	-0.84	-1.9	0.43	0.35	0.28	-0.94	-1.84	0.44	0.9	-0.44	1.56	-1.29	0.53	0.91	1.41
IPSLCM5A	-0.66	-1.93	0.43	0.01	0.83	-0.36	-1.81	0.65	0.93	-0.13	1.67	-1.31	0.6	1.59	0.79
MPIESM12	-0.91	-1.66	0.71	0.33	-0.29	-1.19	-1.9	0.6	0.99	-0.89	1.22	-1.35	0.77	1.22	0.57
mean	-0.84	-1.75	0.61	0.24	0.06	-0.86	-1.88	0.7	0.64	-0.32	0.87	-1.34	0.74	1.14	0.33
mean (no GISSE2R)	-0.76	-1.79	0.64	0.21	0.18	-0.82	-1.9	0.73	0.68	-0.33	1.2	-1.34	0.8	1.21	0.53
change															
CESM104	0.7	0.08	0.13	0.06	0.42	-0.02	-0.0	0.01	-0.0	-0.02	-0.0	-0.1	0.27	-0.29	0.12
CNRMCM61	0.3	0.17	-0.26	-0.02	0.41	0.0	0.0	0.01	-0.0	0.0	0.02	0.04	0.07	0.07	-0.16
GISSE2R	1.23	0.31	0.02	0.15	0.75	0.02	-0.0	0.01	-0.01	0.03	0.17	-0.08	0.06	0.01	0.19
HadCM3L	0.67	0.04	-0.0	-0.17	0.81	-0.01	-0.0	-0.01	-0.0	-0.0	0.1	0.01	0.08	0.01	-0.0
IPSLCM5A	0.22	0.09	-0.12	-0.06	0.3	0.01	0.0	0.0	-0.0	0.0	-0.2	-0.04	0.08	-0.12	-0.12
MPIESM12	0.81	0.18	0.1	-0.07	0.59	0.01	-0.0	0.01	0.0	0.0	-0.38	-0.08	0.17	-0.11	-0.37
mean	0.65	0.14	-0.02	-0.02	0.55	0.0	-0.0	0.0	-0.0	0.0	-0.05	-0.04	0.12	-0.07	-0.06
mean (no GISSE2R)	0.54	0.11	-0.03	-0.05	0.51	-0.0	-0.0	0.0	-0.0	-0.0	-0.09	-0.03	0.13	-0.09	-0.1

Table S8: Full, local, and nonlocal feedbacks estimated using the MR method for all models and flux components. GISSE2R is the only model that exhibits a negative local or positive nonlocal feedback, due to its cloud feedbacks, which are out of keeping with observational results (see Section 4). Multi-model means with or without GISSE2R show large compensating local and nonlocal feedbacks, particularly due to the SW cloud feedback, which appears to be anti-correlated between models (local and nonlocal SW cloud columns). The correlation coefficient for early period non-GISSE2R local vs. nonlocal feedbacks is -0.96, and for late is -0.98. All feedbacks have units of $Wm^{-2}K^{-1}$.

	MR					MR (local)					MR (nonlocal)				
model	net	LW clear	SW clear	LW cloud	SW cloud	net	LW clear	SW clear	LW cloud	SW cloud	net	LW clear	SW clear	LW cloud	SW cloud
early															
CESM104	-0.56	-1.89	1.12	0.3	-0.09	3.51	-1.29	1.1	0.67	3.04	-4.07	-0.59	0.02	-0.37	-3.13
CNRMCM61	-0.65	-1.87	0.98	0.38	-0.13	1.43	-1.64	1.05	-0.53	2.56	-2.08	-0.23	-0.07	0.91	-2.68
GISSE2R	-1.36	-1.84	0.55	0.31	-0.39	-1.93	-1.28	0.51	0.01	-1.16	0.57	-0.56	0.04	0.3	0.78
HadCM3L	-1.46	-2.12	0.43	0.48	-0.24	4.0	-1.35	0.49	-0.16	5.01	-5.45	-0.78	-0.06	0.63	-5.25
IPSLCM5A	-0.52	-2.03	0.64	0.33	0.54	4.12	-1.0	0.6	1.51	3.01	-4.64	-1.03	0.04	-1.18	-2.46
MPIESM12	-1.01	-1.83	0.72	0.58	-0.49	3.82	-1.1	0.66	1.5	2.75	-4.83	-0.73	0.06	-0.92	-3.24
mean	-0.93	-1.93	0.74	0.4	-0.13	2.49	-1.28	0.74	0.5	2.53	-3.42	-0.65	0.01	-0.1	-2.66
mean (no GISSE2R)	-0.84	-1.95	0.78	0.41	-0.08	3.37	-1.28	0.78	0.6	3.27	-4.21	-0.67	-0.0	-0.18	-3.35
late															
CESM104	-0.37	-1.85	1.41	0.29	-0.23	3.04	-1.27	1.51	1.07	1.74	-3.41	-0.58	-0.09	-0.78	-1.96
CNRMCM61	-0.47	-1.87	1.03	0.34	0.04	1.58	-1.57	1.15	-0.35	2.36	-2.05	-0.29	-0.12	0.69	-2.33
GISSE2R	-0.86	-1.71	0.69	0.37	-0.21	-0.41	-1.21	0.77	0.58	-0.55	-0.45	-0.5	-0.08	-0.21	0.34
HadCM3L	-0.84	-2.09	0.51	0.25	0.5	3.91	-1.31	0.6	0.18	4.43	-4.75	-0.78	-0.1	0.07	-3.94
IPSLCM5A	-0.32	-1.97	0.79	0.24	0.61	3.72	-1.03	0.69	1.5	2.57	-4.05	-0.94	0.11	-1.26	-1.96
MPIESM12	-0.81	-1.78	0.91	0.36	-0.3	3.39	-1.17	0.86	1.43	2.27	-4.2	-0.61	0.04	-1.07	-2.57
mean	-0.61	-1.88	0.89	0.31	0.07	2.54	-1.26	0.93	0.74	2.14	-3.15	-0.62	-0.04	-0.43	-2.07
mean (no GISSE2R)	-0.56	-1.91	0.93	0.3	0.12	3.13	-1.27	0.96	0.77	2.67	-3.69	-0.64	-0.03	-0.47	-2.55
change															
CESM104	0.19	0.04	0.3	-0.01	-0.13	-0.47	0.02	0.41	0.4	-1.3	0.65	0.02	-0.11	-0.42	1.17
CNRMCM61	0.18	0.01	0.05	-0.04	0.16	0.15	0.07	0.1	0.18	-0.19	0.03	-0.06	-0.05	-0.21	0.36
GISSE2R	0.51	0.12	0.14	0.07	0.18	1.52	0.07	0.26	0.58	0.61	-1.01	0.06	-0.12	-0.51	-0.44
HadCM3L	0.61	0.04	0.07	-0.23	0.74	-0.09	0.04	0.11	0.34	-0.57	0.7	-0.0	-0.04	-0.57	1.31
IPSLCM5A	0.2	0.06	0.16	-0.09	0.07	-0.4	-0.03	0.08	-0.01	-0.44	0.59	0.09	0.07	-0.08	0.51
MPIESM12	0.21	0.05	0.18	-0.22	0.19	-0.42	-0.07	0.2	-0.07	-0.48	0.63	0.12	-0.02	-0.15	0.67
mean	0.31	0.05	0.15	-0.09	0.2	0.05	0.02	0.19	0.24	-0.4	0.27	0.04	-0.04	-0.32	0.6
mean (no GISSE2R)	0.28	0.04	0.15	-0.12	0.21	-0.24	0.0	0.18	0.17	-0.6	0.52	0.03	-0.03	-0.29	0.8

2 Figures

2.1 Conceptual model with noise at TOA instead of surface

The conceptual model used to demonstrate the MR method has two pairs of forcing terms, one at the surface ($\vec{F}_{surf} = \begin{bmatrix} F_{surf,1} \\ F_{surf,2} \end{bmatrix}$)

and one at the top of atmosphere ($\vec{F}_{TOA} = \begin{bmatrix} F_{TOA,1} \\ F_{TOA,2} \end{bmatrix}$):

$$\vec{c}\frac{d\vec{T}'}{dt} = \vec{N} + \begin{bmatrix} \gamma & -\gamma \\ -\gamma & \gamma \end{bmatrix} \vec{T}' + \vec{F}_{surf} \tag{1}$$

$$\vec{N} = \Lambda\vec{T}' + \vec{F}_{TOA} \tag{2}$$

Forcing at the surface generates variability from which it is easy to diagnose radiative feedbacks, because N simply follows T via Λ, so that a regression with no lag will recreate Λ. However, forcing at the TOA creates two different relationships: T follows N positively because a net energy flux warms the planet, while N follows T typically negatively because of radiative feedbacks. These two influences reach a balance in which the regression of N against T changes depending on the lag between them, with no correlation occurring at zero lag. For the real climate, and for climate models, noise occurs at both levels, so that regression without lag tends to produce estimates of radiative feedbacks somewhere between the true value and zero (Spencer and Braswell, 2008, 2011; Choi et al., 2014; Proistosescu et al., 2018).

We can see this concretely if we rerun the example from the text, but with the variance of F_{surf} and F_{TOA} being 10 and 15 Wm^{-2} instead of 20 and 5 Wm^{-2}:
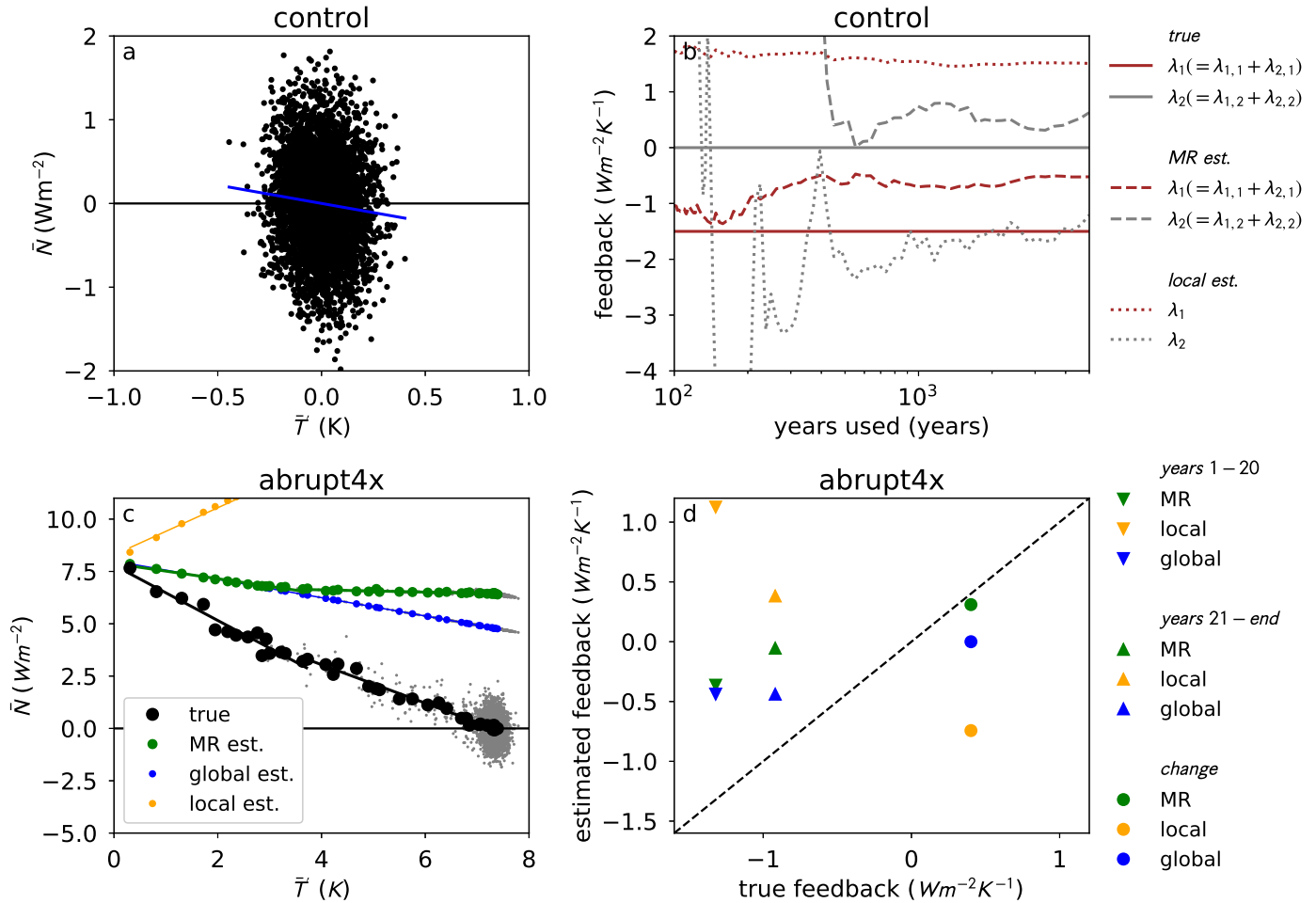
Figure S1: Conceptual model with stochastic forcing shifted from surface to TOA.

With these noise terms, the regression of $\bar{N}$ vs $\bar{T}'$ is shifted flatter (panel a) and MR estimates of λ_2 are shifted towards zero (panel b). As a result the global and MR estimates of the abrupt4x feedbacks are shifted towards zero as well (panels c and d). The shift tends to be proportional, so that the difference between feedbacks in the early and late period are reduced (circle markers in panel d).

2.2 Feedbacks vs. time for component fluxes
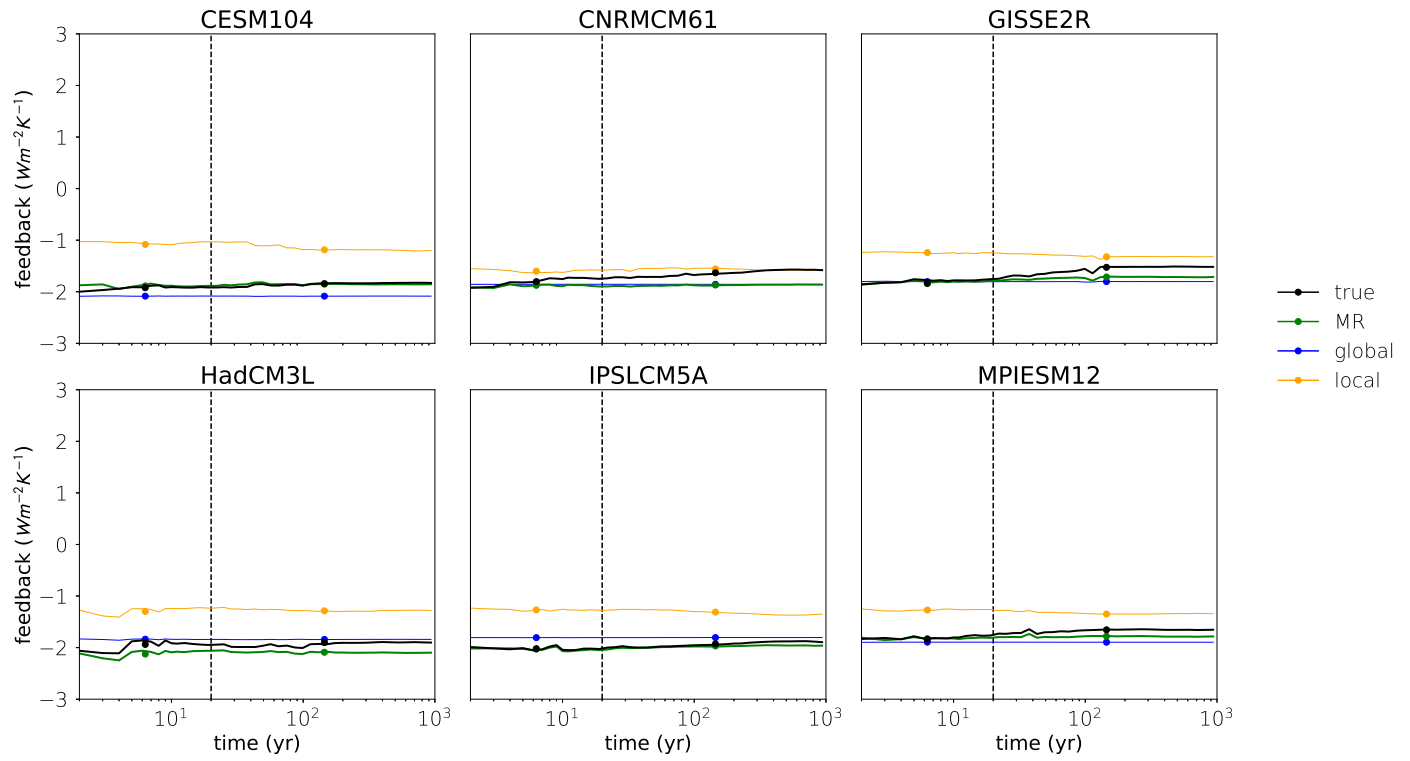
Figure S2: Like Figure 5 in the main body of the text, but for the LW clear feedback.
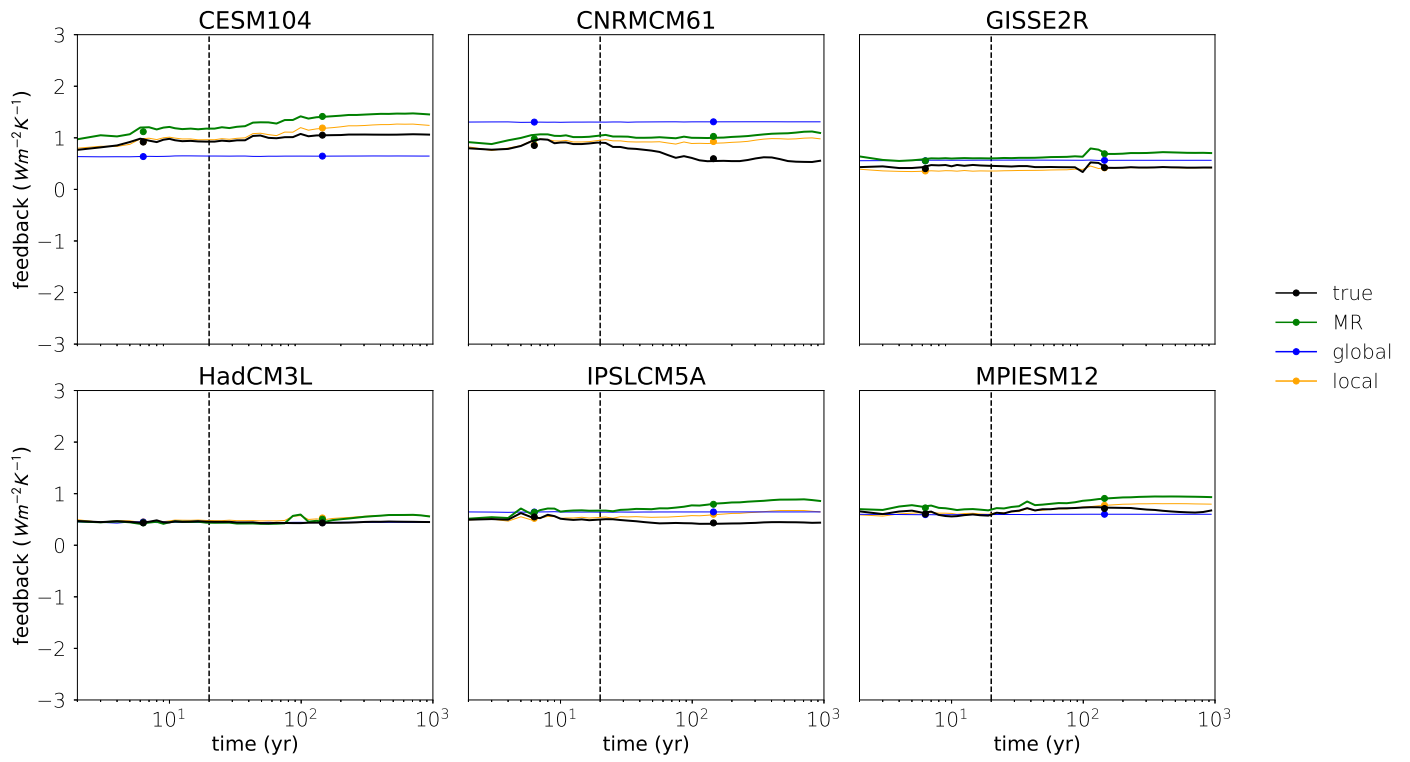
Figure S3: Like Figure 5 in the main body of the text, but for the SW clear feedback.
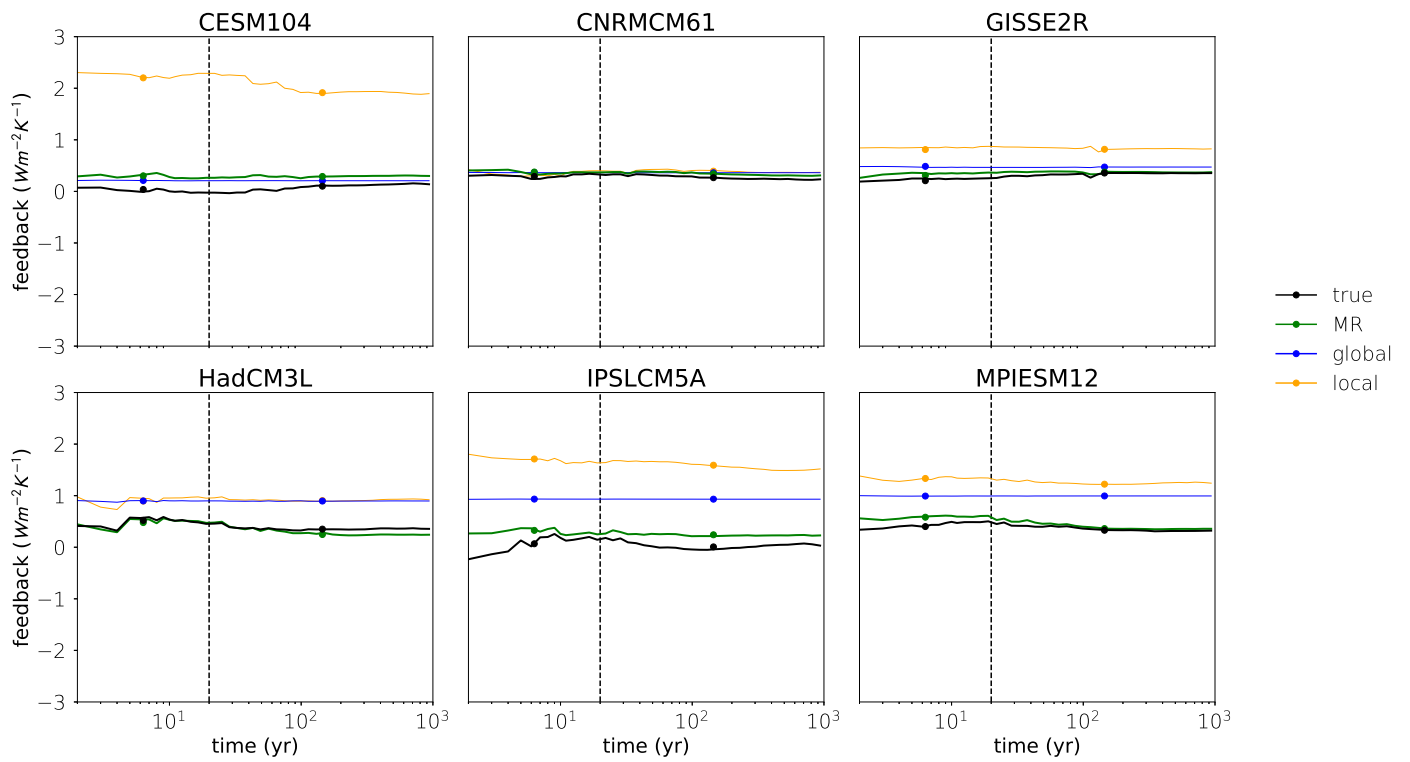
Figure S4: Like Figure 5 in the main body of the text, but for the LW cloud feedback.
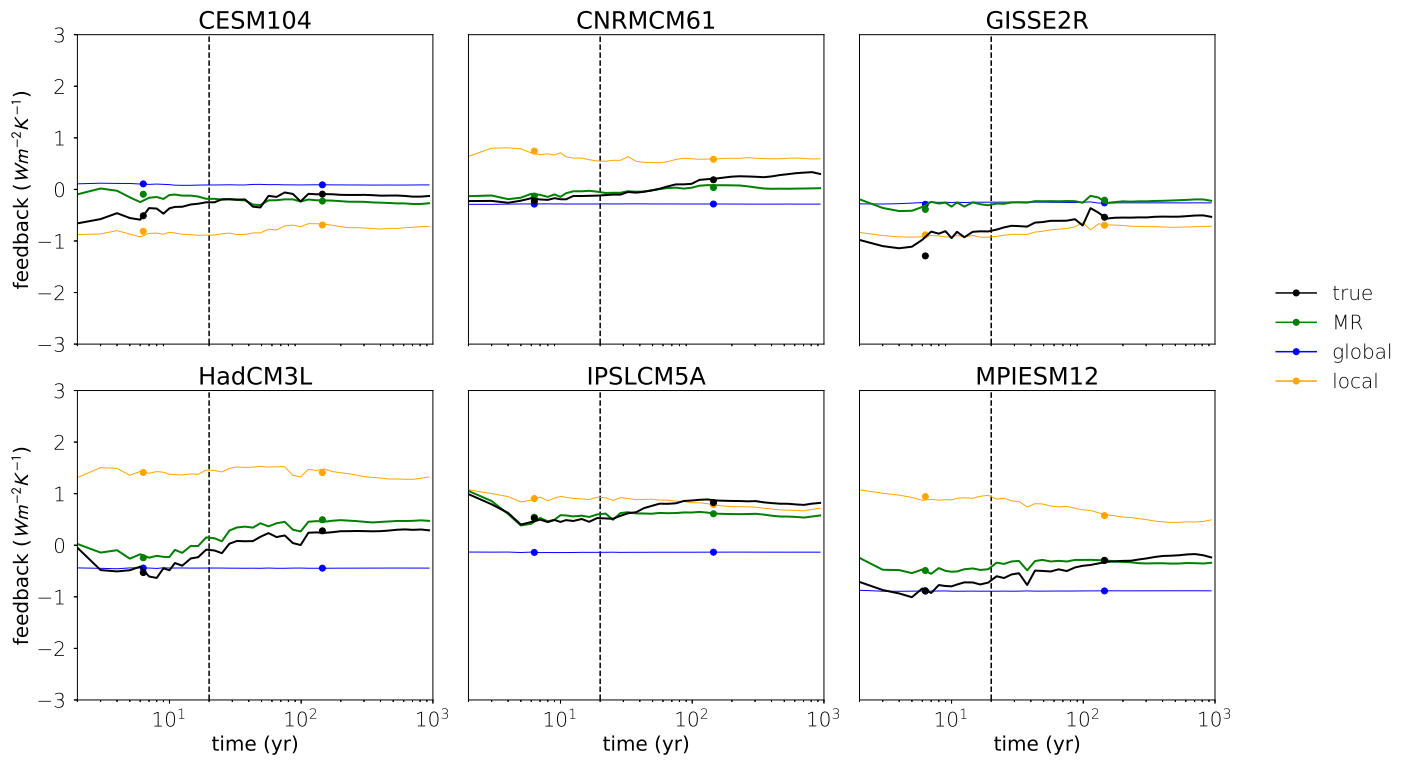
Figure S5: Like Figure 5 in the main body of the text, but for the SW cloud feedback.

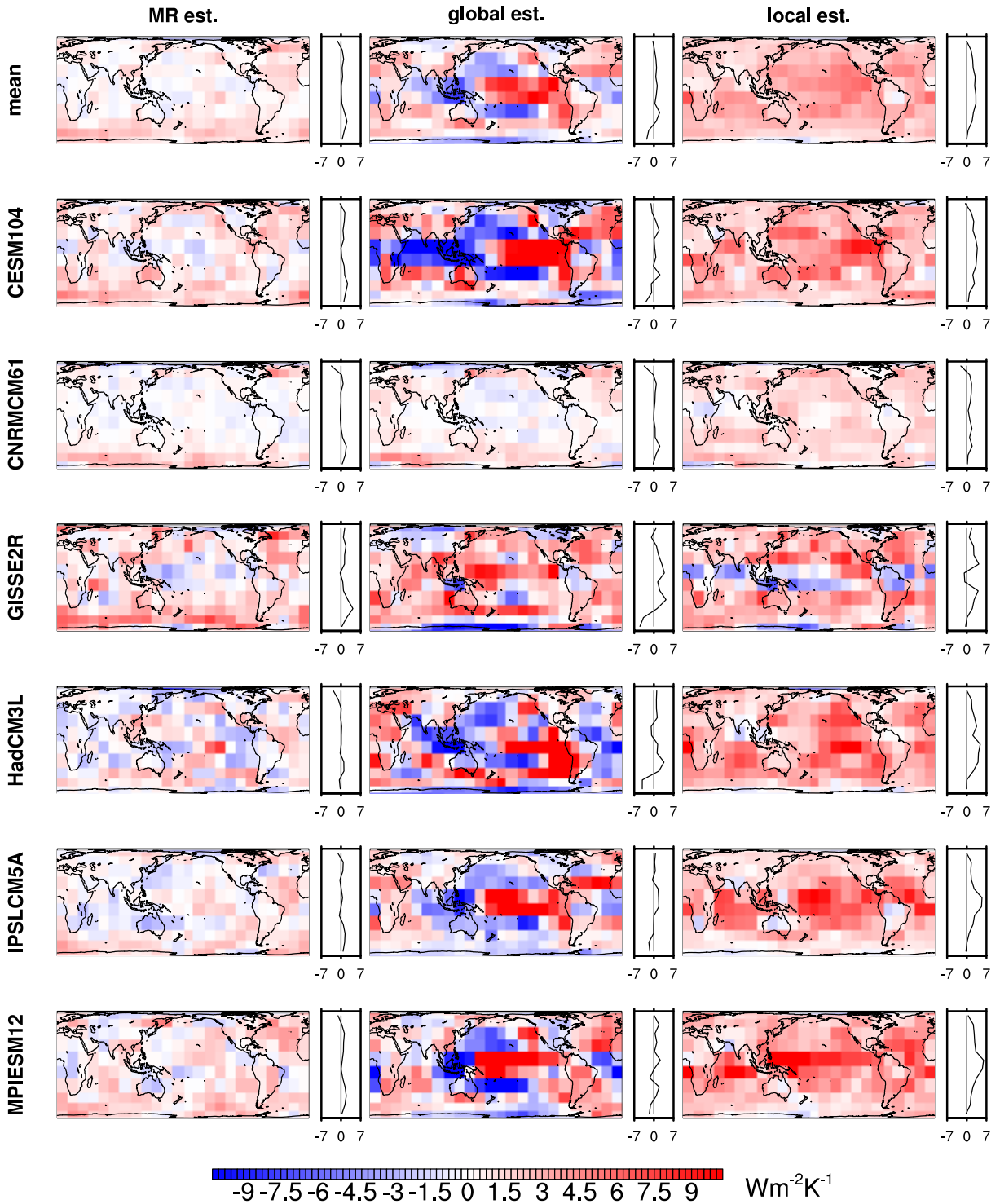## 2.3 Spatial patterns of normalized changes in top-of-atmosphere flux

2.3.1 Errors and individual models

Figure S6: Error (estimated value - true value) for the normalized spatial pattern of net TOA flux change during the early period for the multi-model mean (Fig. 7) and component models, with zonal means to the right of each panel. The MR method has the smallest spatial error (Table S4). The MR method overestimates the change over the Southern Ocean and the north Atlantic in all models, and experiences cancelling errors of a similar sign in the tropics for GISSE2R, HadCM3L, and IPSLCM5A.
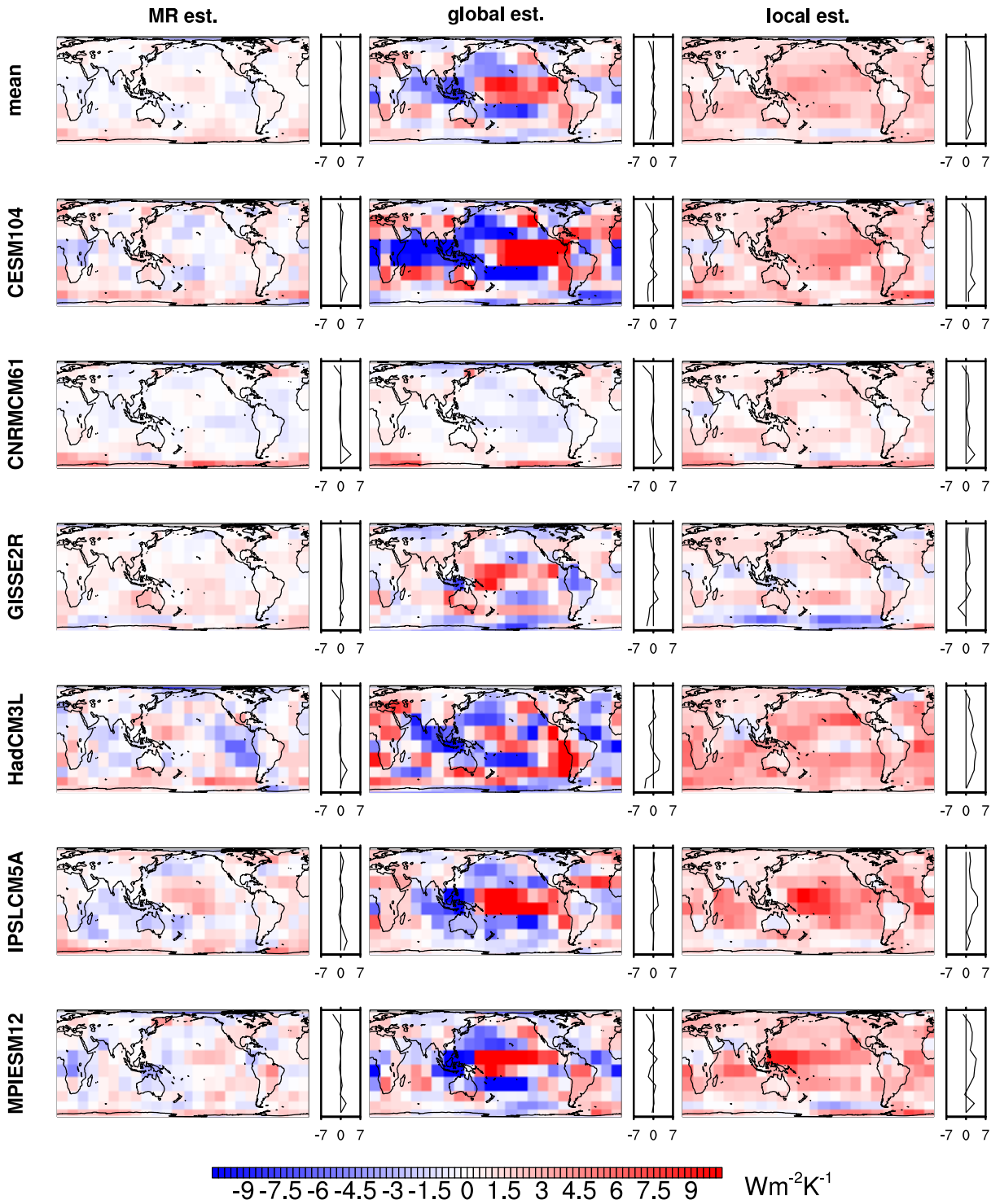
Figure S7: Same as Figure S6, except instead of showing results for the early period, this shows results for the late period. Once more, the MR method has the smallest spatial error (Table S4), and the MR method errors tend to be smaller than for the early period.
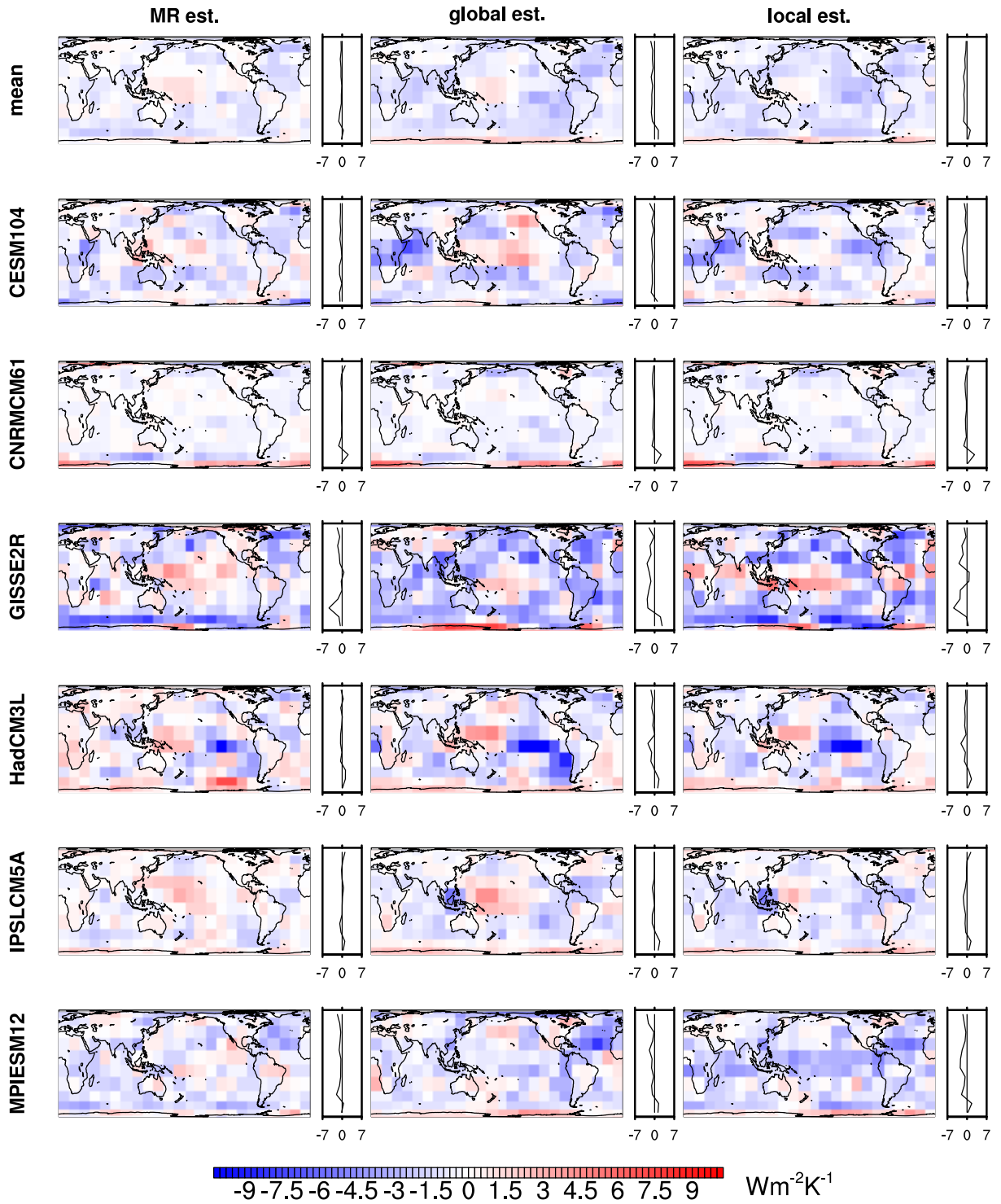
Figure S8: Same as Figure S6, except instead of showing results for the early period, this shows results for the difference between the early and late periods. Once more, the MR method has the smallest spatial error (Table S4).

2.3.2 Component fluxes
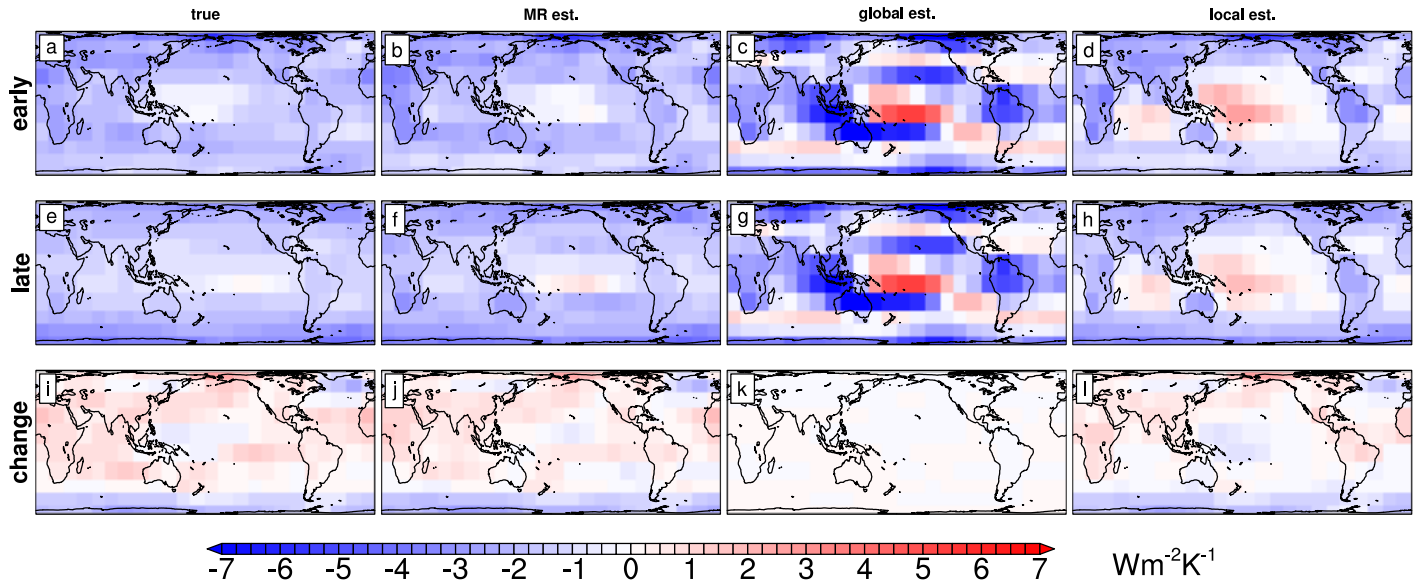
Figure S9: Like Figure 7 in the main body of the paper, but for the LW clear feedback The MR and true patterns show a lot of agreement (see Figure S14 for the difference between the estimates and true values).
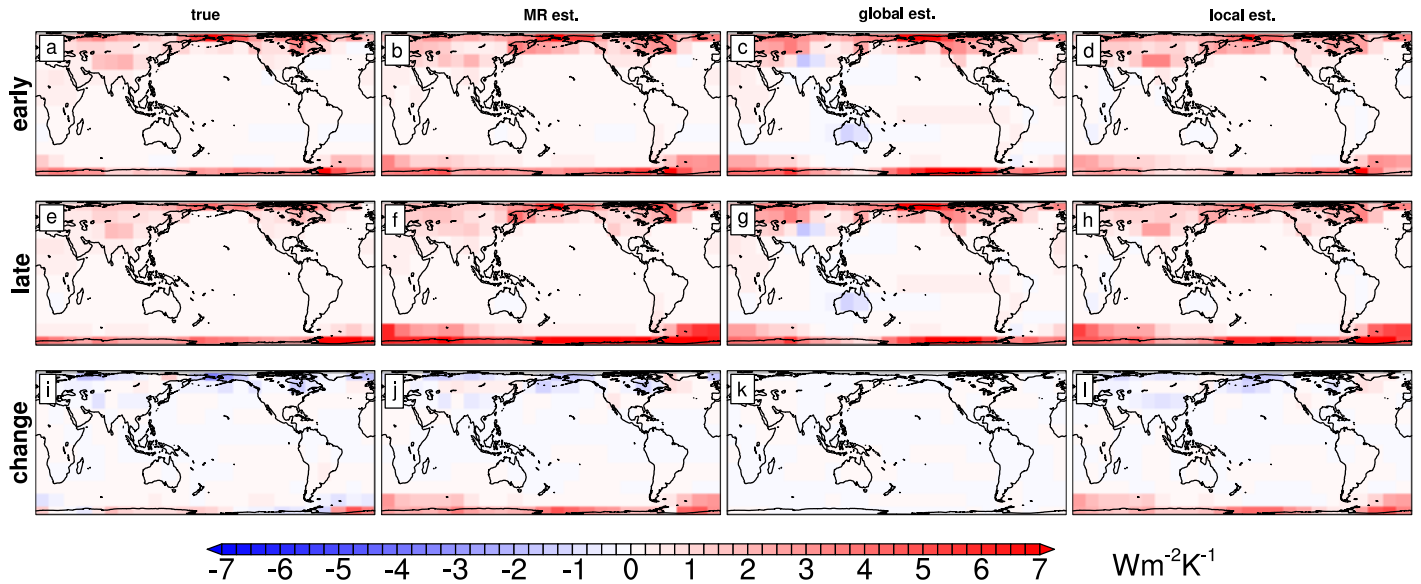
Figure S10: Like Figure 7 in the main body of the paper, but for the SW clear feedback. Since the biggest SW clear feedback is the predominantly local ice albedo feedback, both the local and MR methods both capture the true pattern well (see Figure S15 for the difference between the estimates and true values).
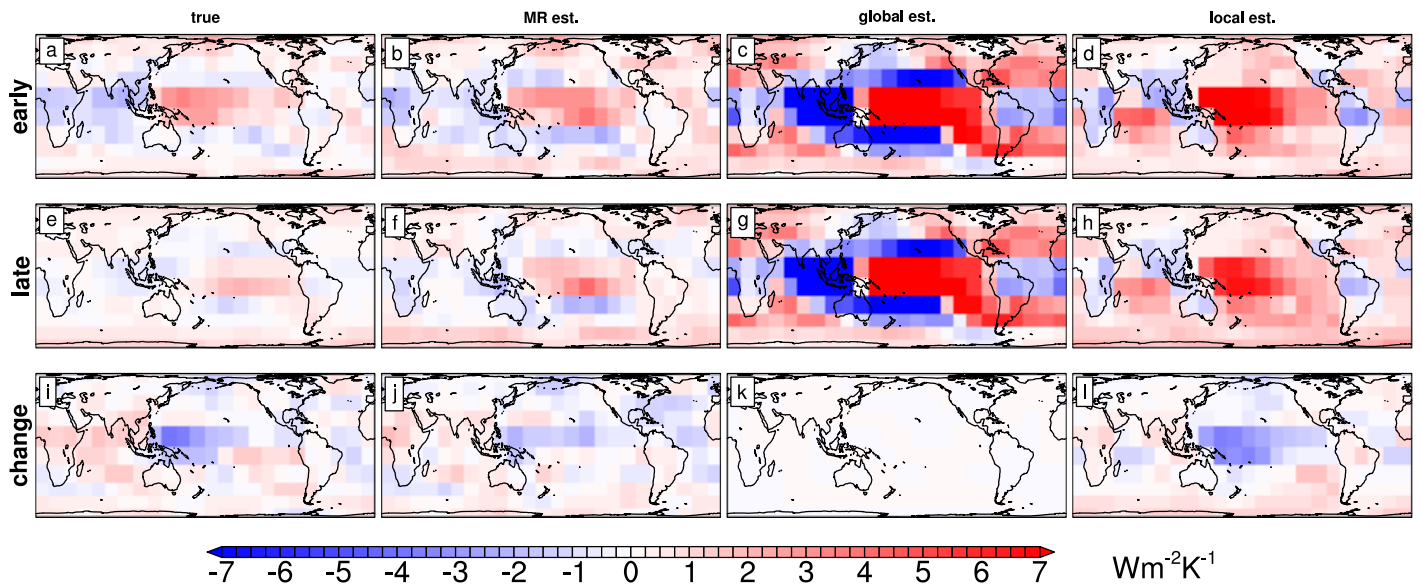
Figure S11: Like Figure 7 in the main body of the paper, but for the LW cloud feedback. The MR method does well in most regions (see Figure S16 for the difference between the estimates and true values).
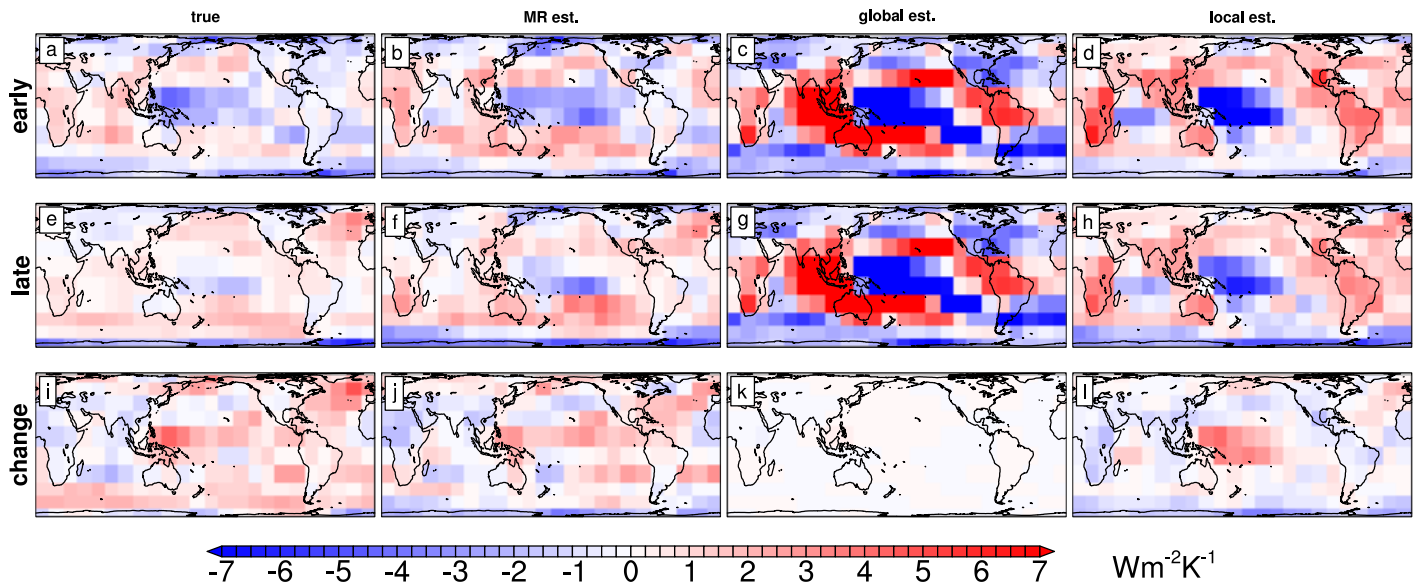
Figure S12: Like Figure 7 in the main body of the paper, but for the SW cloud feedback. While the MR method captures many features of the true pattern, it appears to overestimate the change in some regions, as shown more fully in Figure S17.

2.3.3 Component flux errors and uncertainty
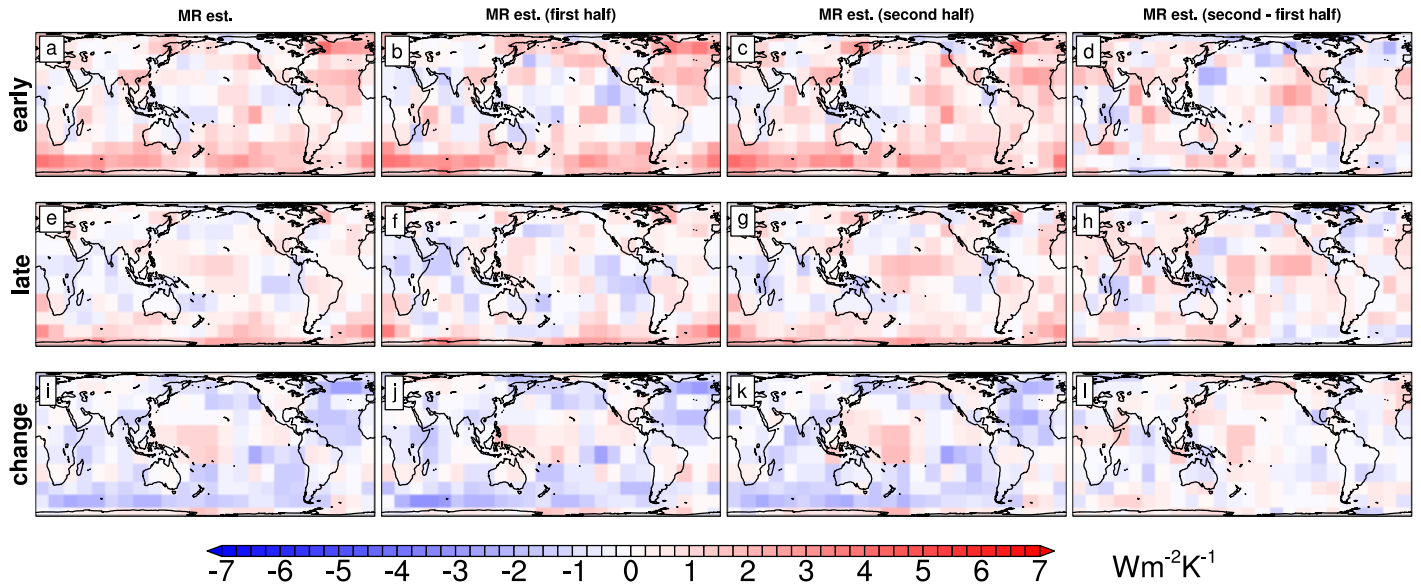
Figure S13: Like Figure 7 in the main body of the paper, but with the true spatial change (the left column of Figure 7) subtracted from the other columns, leaving the errors in the difference. The MR method has an overestimate south of 30°S, as well as in the North Atlantic in the early period. We also include estimates made using just the first and second half of each model's control simulation, and their difference, as a rough test of uncertainty.
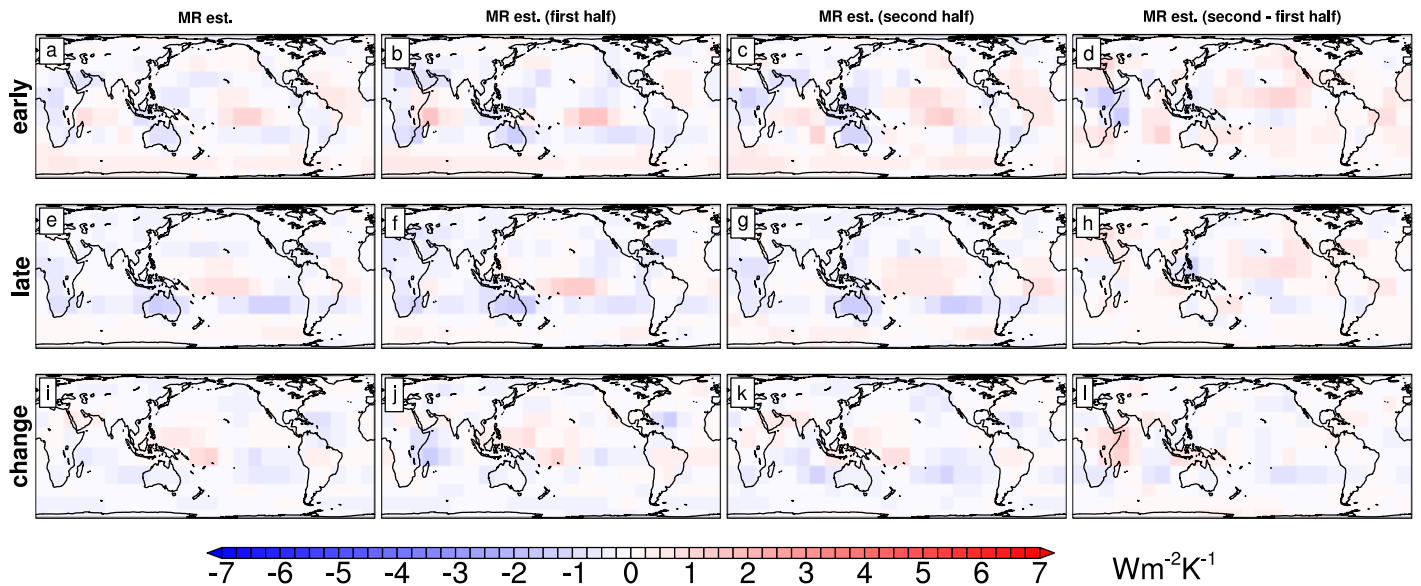
Figure S14: Like Figure S13, but for LW clear. The MR method has no large errors for this feedback.
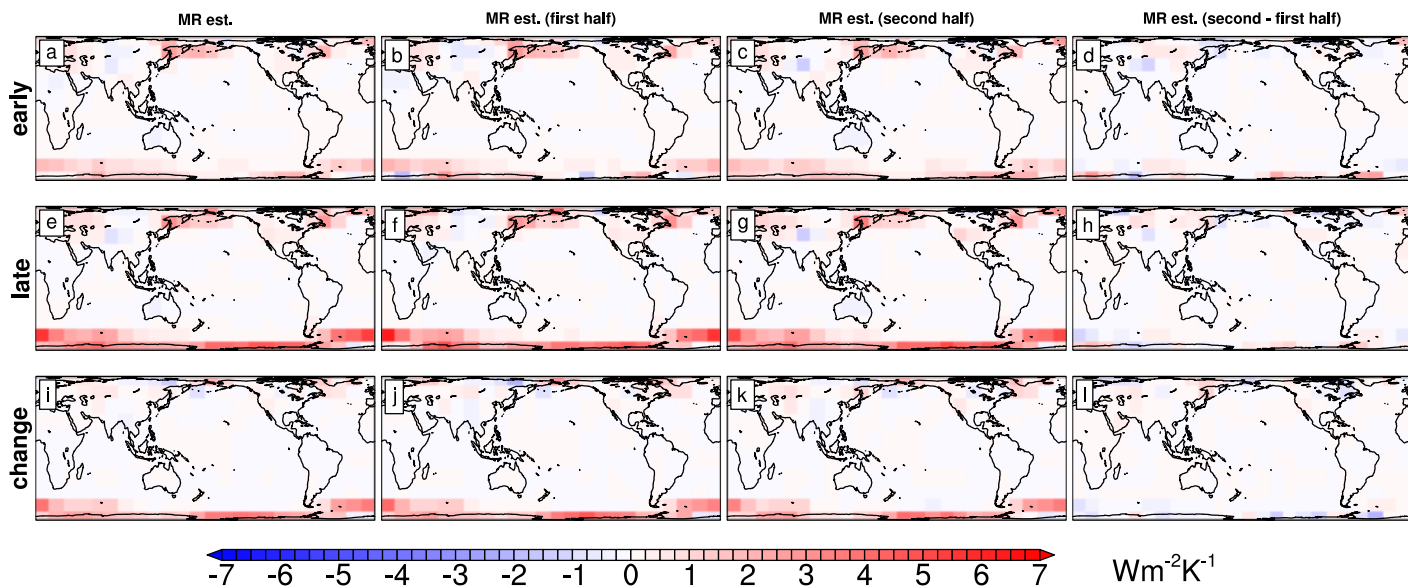
Figure S15: Like Figure S13, but for SW clear. The MR method has some compensating errors between the northern and southern polar regions, with an overestimate south of 60°S.
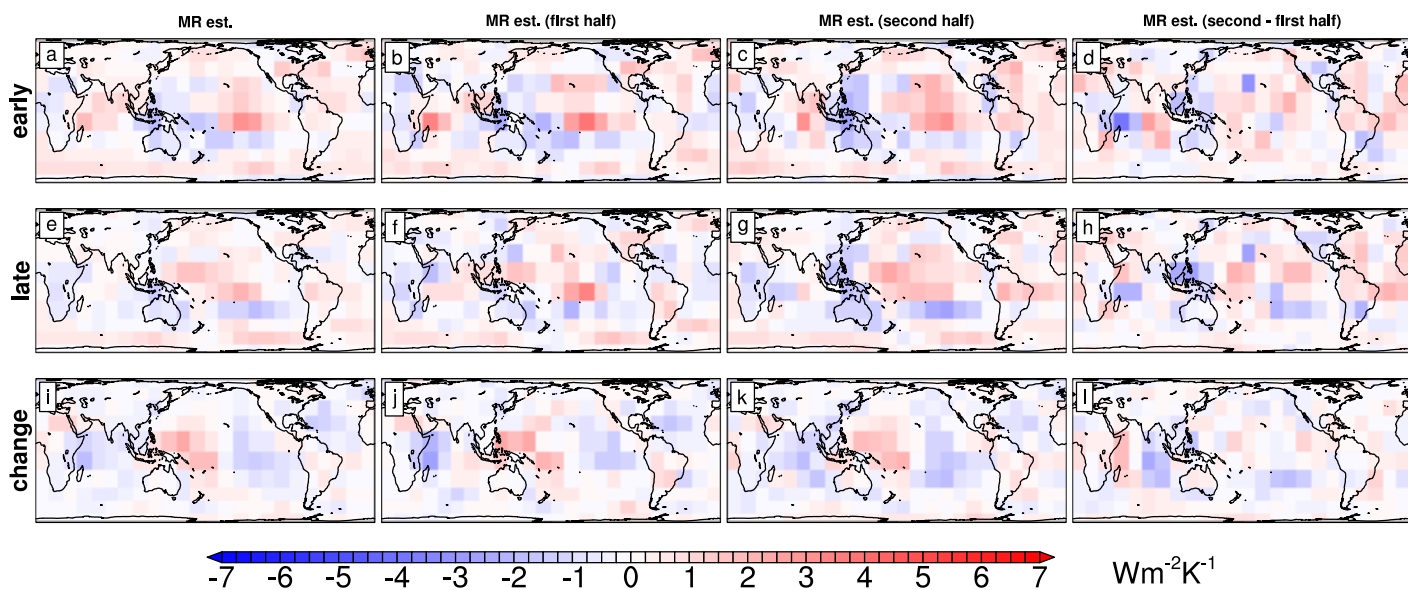
Figure S16: Like Figure S13, but for LW cloud. The MR has a relatively small error, which seems to be anti-correlated with the error in the SW cloud feedback in most regions (Figure S17). The MR method overestimates this feedback in the 45°S-60°S band, contributing to the overestimate south of 30°S.
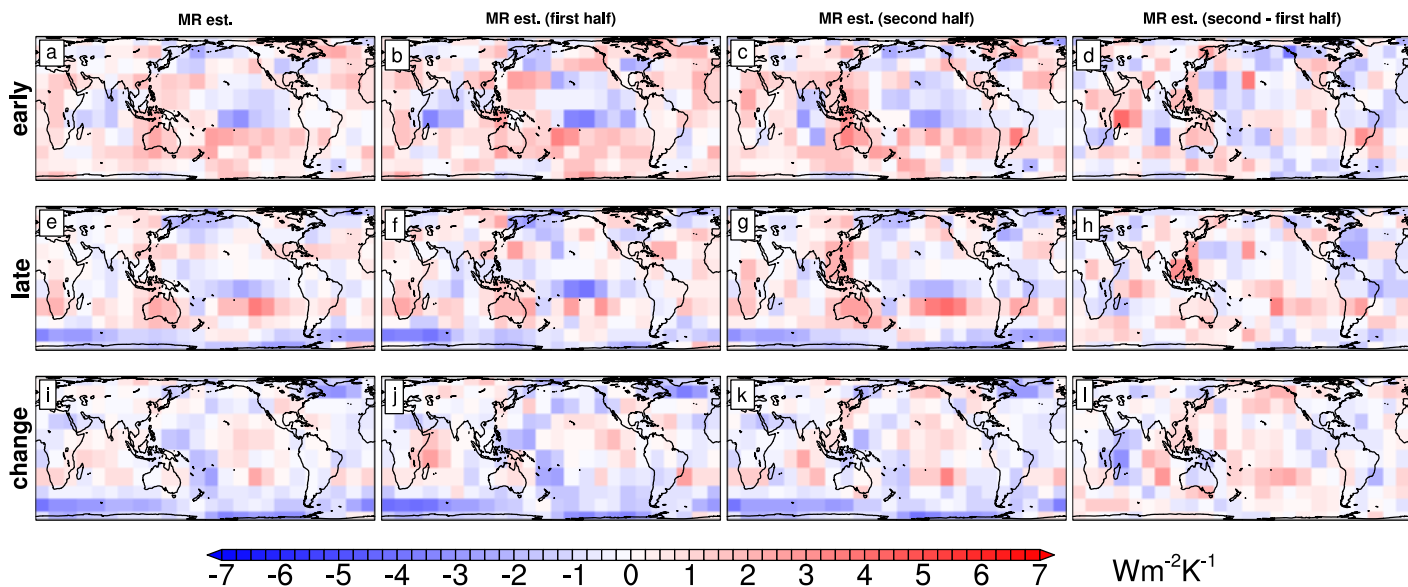
Figure S17: Like Figure S13, but for SW cloud. This feedback has the largest errors for the MR method. Most are offset by errors in the LW cloud feedback (Figure S16), except for between 30°S and 45°S over the Southern Ocean, and during the early period over the North Atlantic. Overestimates in these regions contributed the most to the MR method's overestimate of net feedback (Figures 5 and 6 in the main body of the paper). This component also has the greatest uncertainty.

2.4 Feedbacks

2.4.1 Spatial patterns of feedbacks
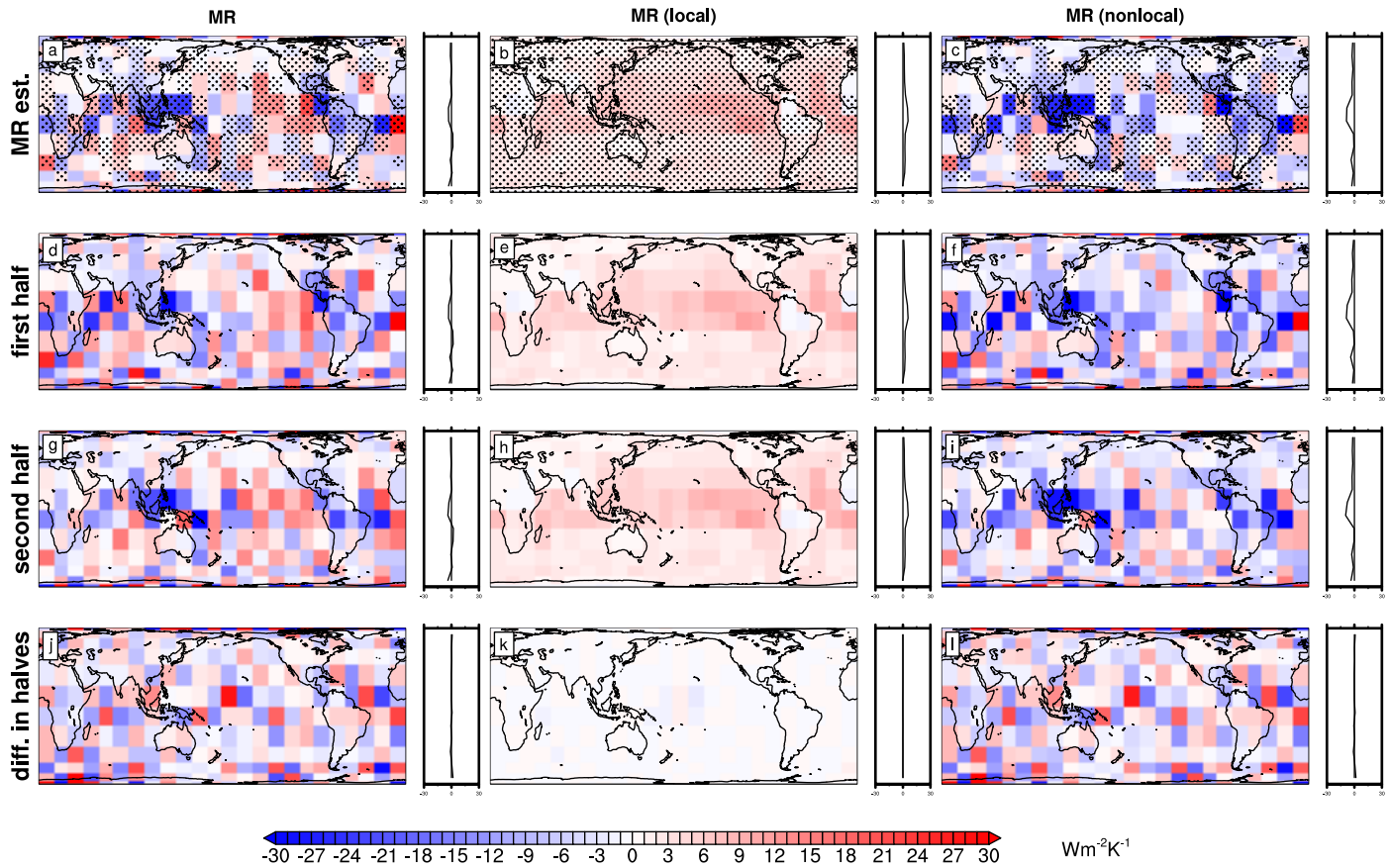
Figure S18: Maps of the spatial pattern of feedbacks estimated by the MR method. The top row is like the top row of Figure 9, and the second and third rows are the same but using only the first and second half of the control simulations respectively. The fourth row is the difference between the second and third rows. The first row has stippling on grid cells where the second and third row agree in sign. It appears to be robust that the local feedback is positive everywhere, and the presence of a nonlocal negative feedback in regions of tropical convection is widely consistent. The nonlocal feedback is quite noisy, although this noise appears to cancel out somewhat in estimates of the spatial pattern of TOA flux change (Figure S13), perhaps because regions which are spatially correlated in the control simulation (allowing large competing feedbacks) are also spatially correlated in the abrupt4x simulations (causing those feedbacks to cancel). Line graphs on the right of each panel show the zonal means of that panel. The zonal averages are robust.
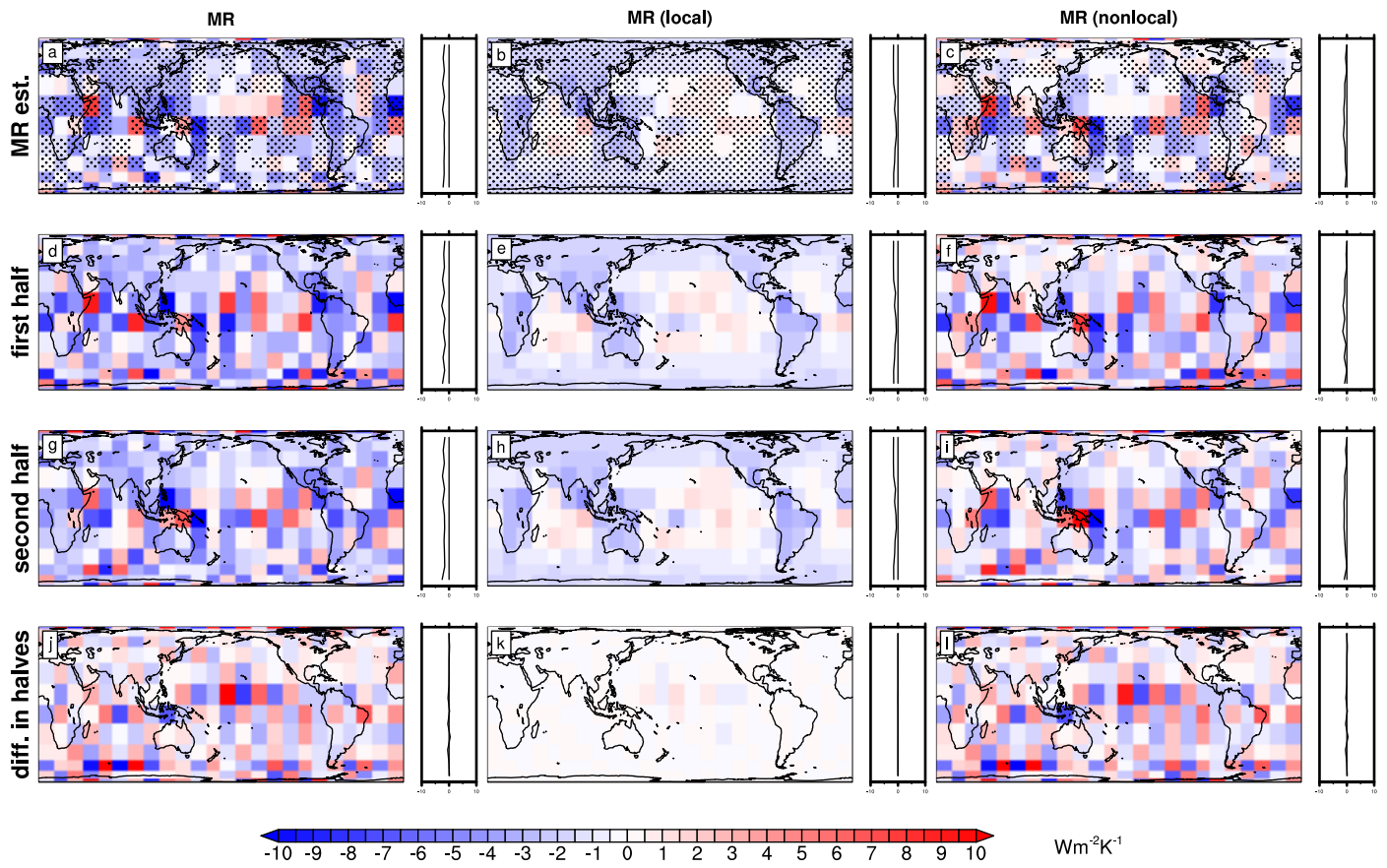
Figure S19: Like Figure S18, but for LW clear. The sign of the local feedback is mostly robust, and the sign of the nonlocal feedback in tropical convecting regions is robust. As with the net feedback, a lot of the noise cancels in predicting the forced response (Figure S14). The zonal averages are robust.
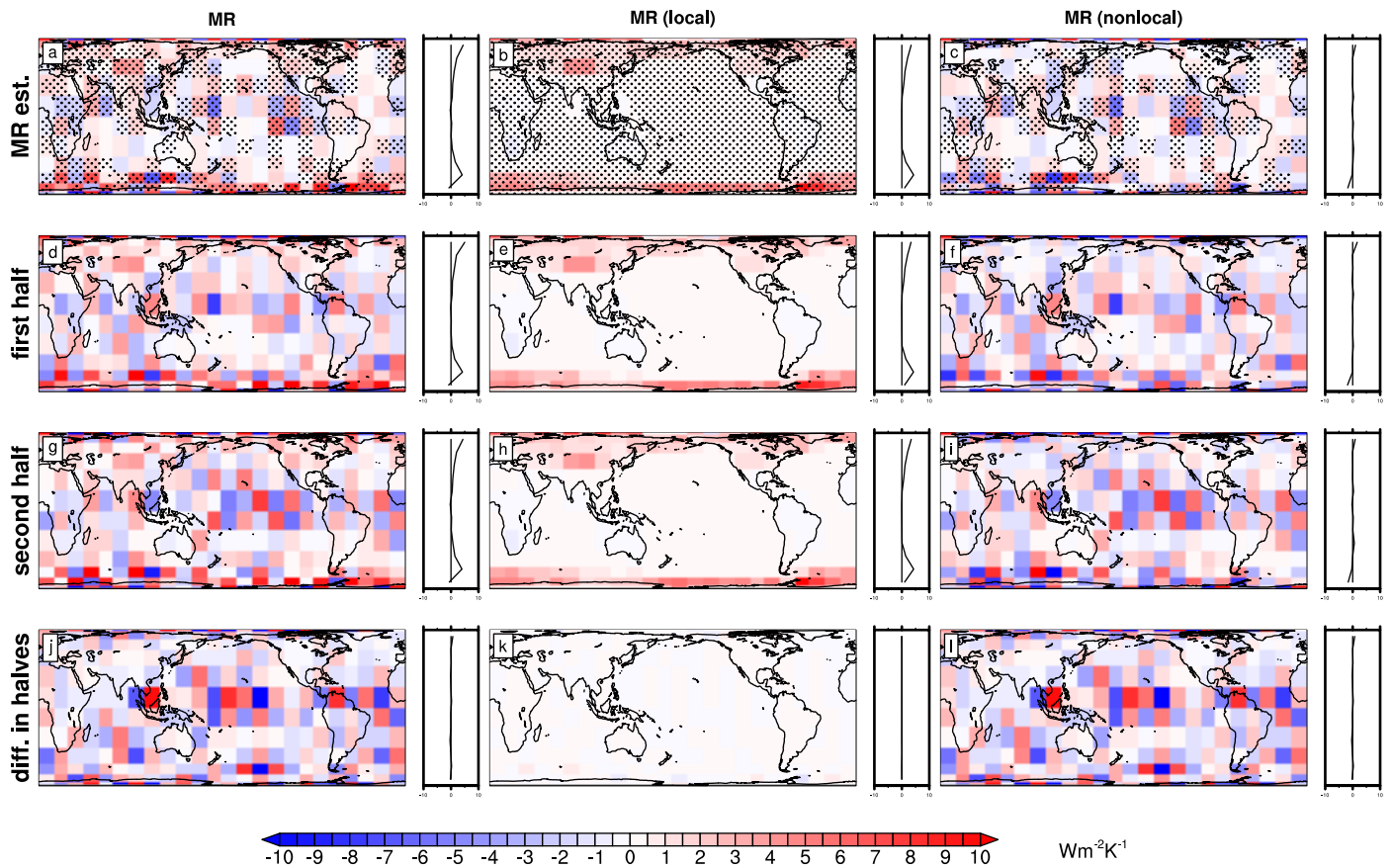
Figure S20: Like Figure S18, but for SW clear. This feedback is primarily local, which is robust in its sign almost everywhere. Its nonlocal feedback is small, and so noise can be much larger than the signal, leading to a less robust nonlocal and/or nonpolar feedback. As with the net feedback, a lot of the noise cancels in predicting the forced response (Figure S15). The zonal averages are robust.
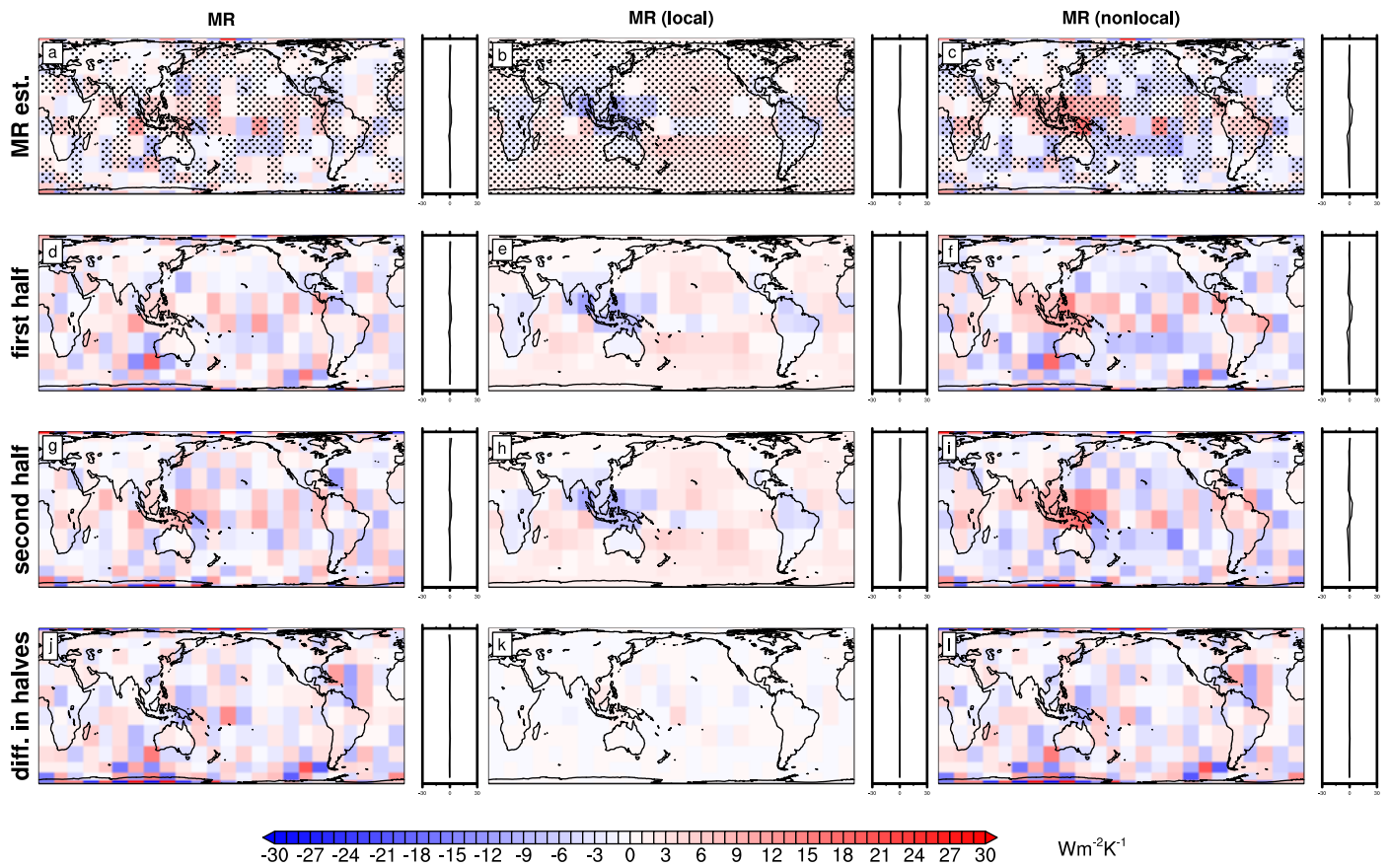
Figure S21: Like Figure S18, but for LW cloud. The local feedback is robust, as is a positive nonlocal feedback in regions of tropical convection. The nonlocal feedback is pretty consistently negative outside of these regions, and while there is some degree of noise, it cancels out somewhat when the spatial pattern of TOA flux is estimated (Figure S16). The zonal averages are robust.
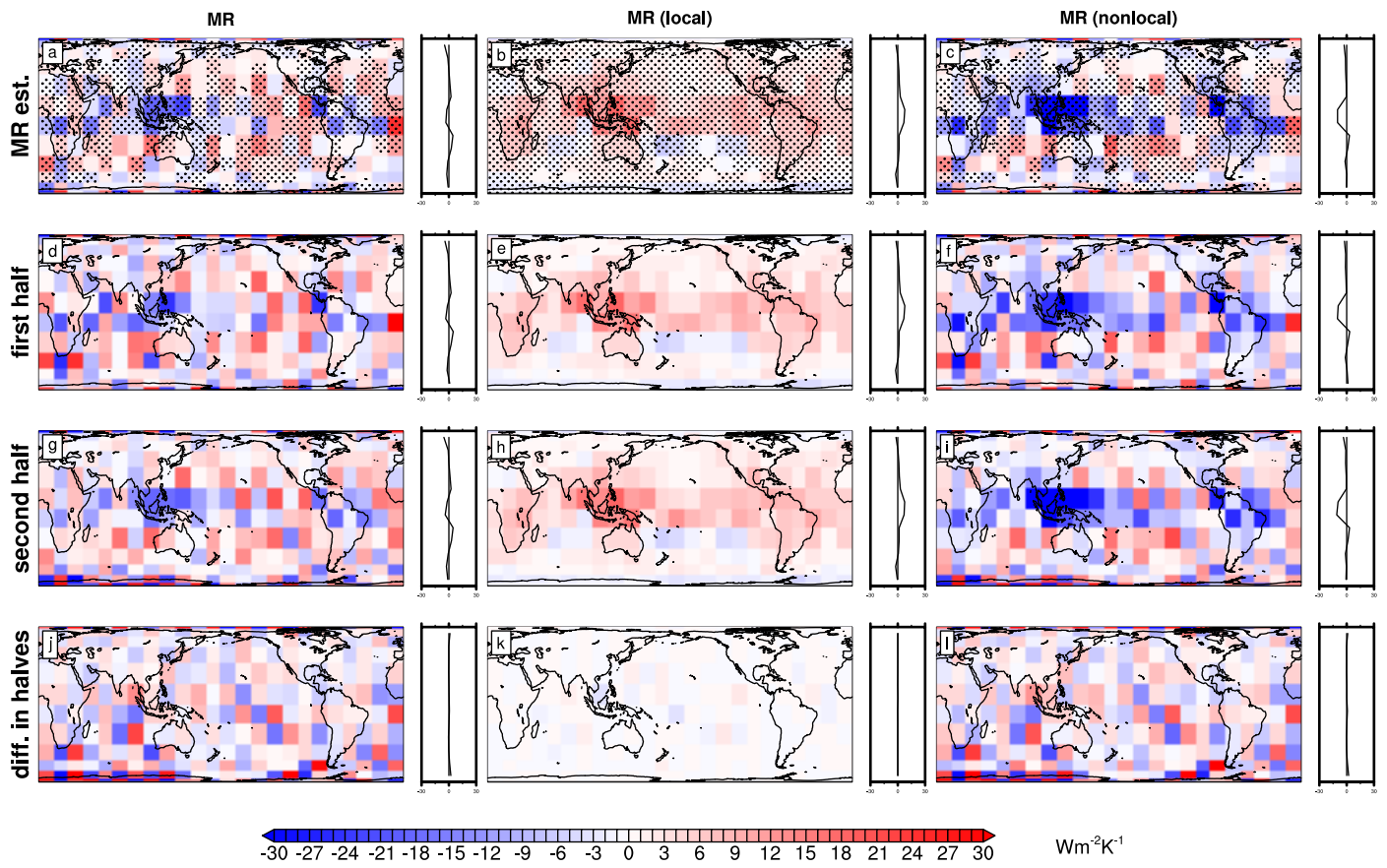
Figure S22: Like Figure S18, but for SW cloud. The local feedback appears to have little uncertainty, as does the nonlocal feedback in regions of tropical convection, and large parts of the extratropics. The zonal averages are robust.
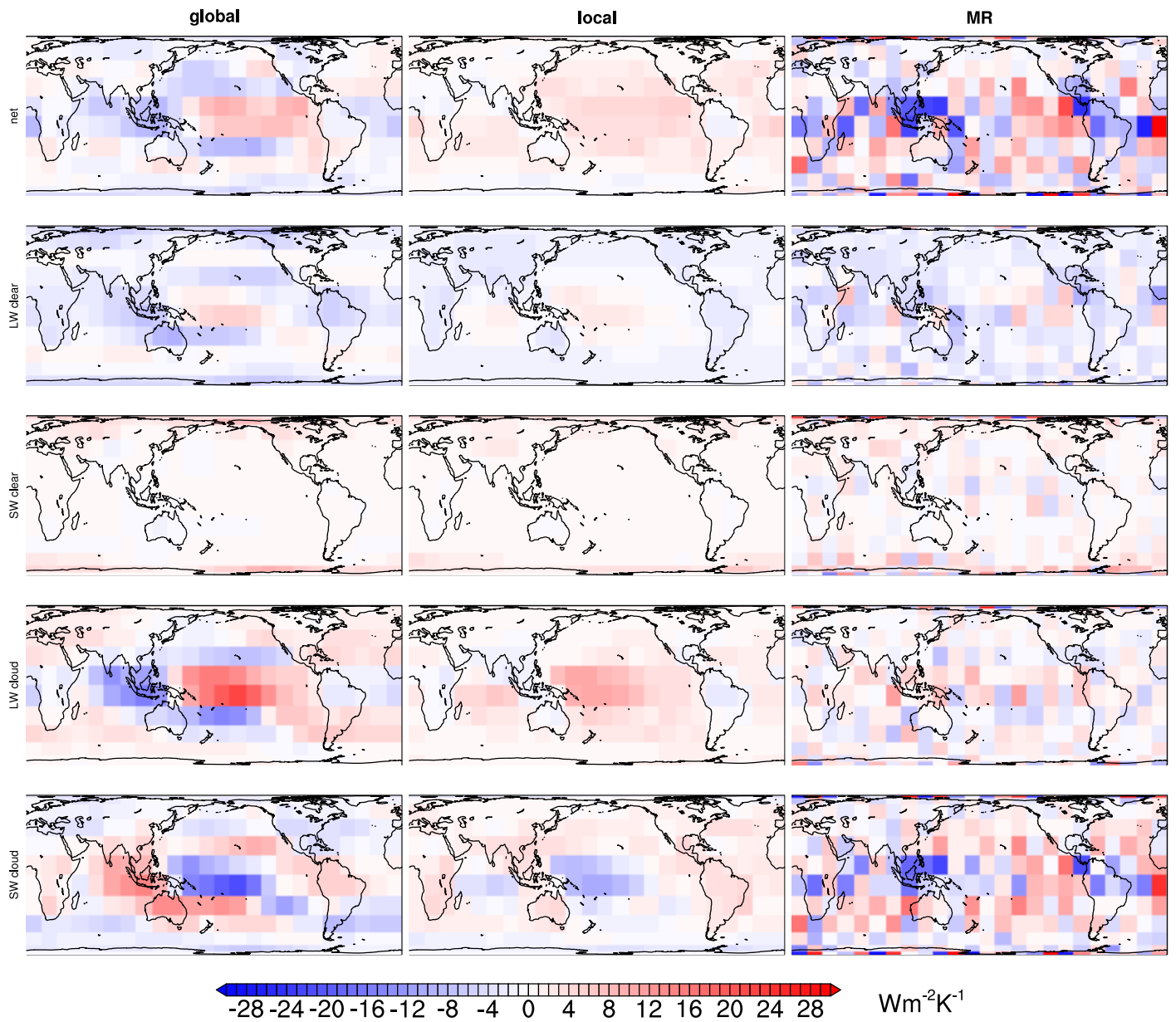
2.4.2 Global and local feedbacks

Figure S23: Multi-model mean of spatial feedbacks estimated using three methods: global (left column), local (middle column), and MR (right column). The net local feedback (top middle panel) resembles the map of spatial feedbacks in Figure 10 of Trenberth et al. (2015), which was made by applying the local method to observations and reanalysis.
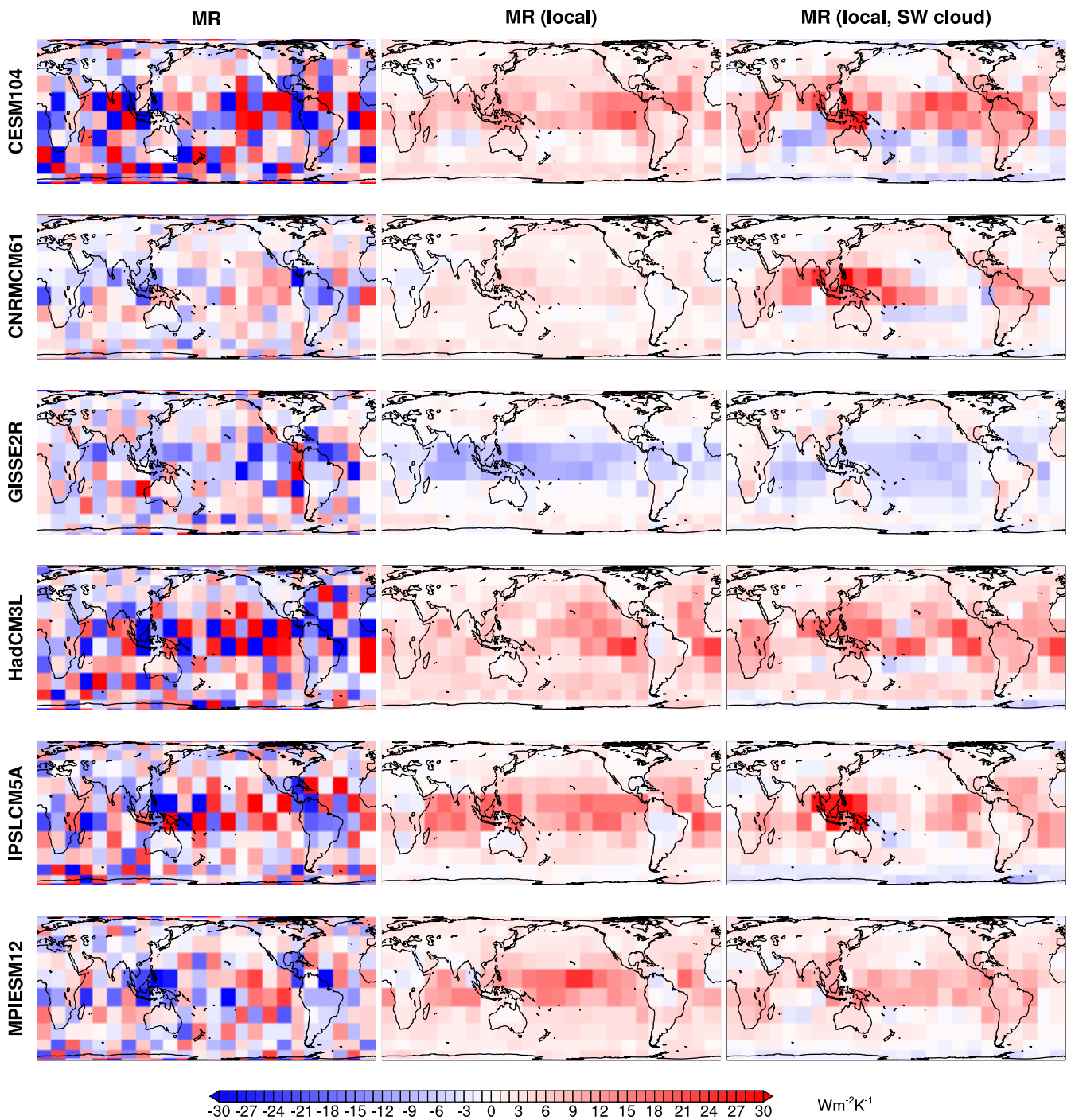
2.4.3 Individual models

Figure S24: Multi-season mean spatial feedbacks estimated by the MR method, as in Figure 9 of the paper, except shown for each model. Feedbacks are qualitatively similar between models, except for GISSE2R, which is missing the positive local SW cloud feedback in tropical convecting regions seen in other models.
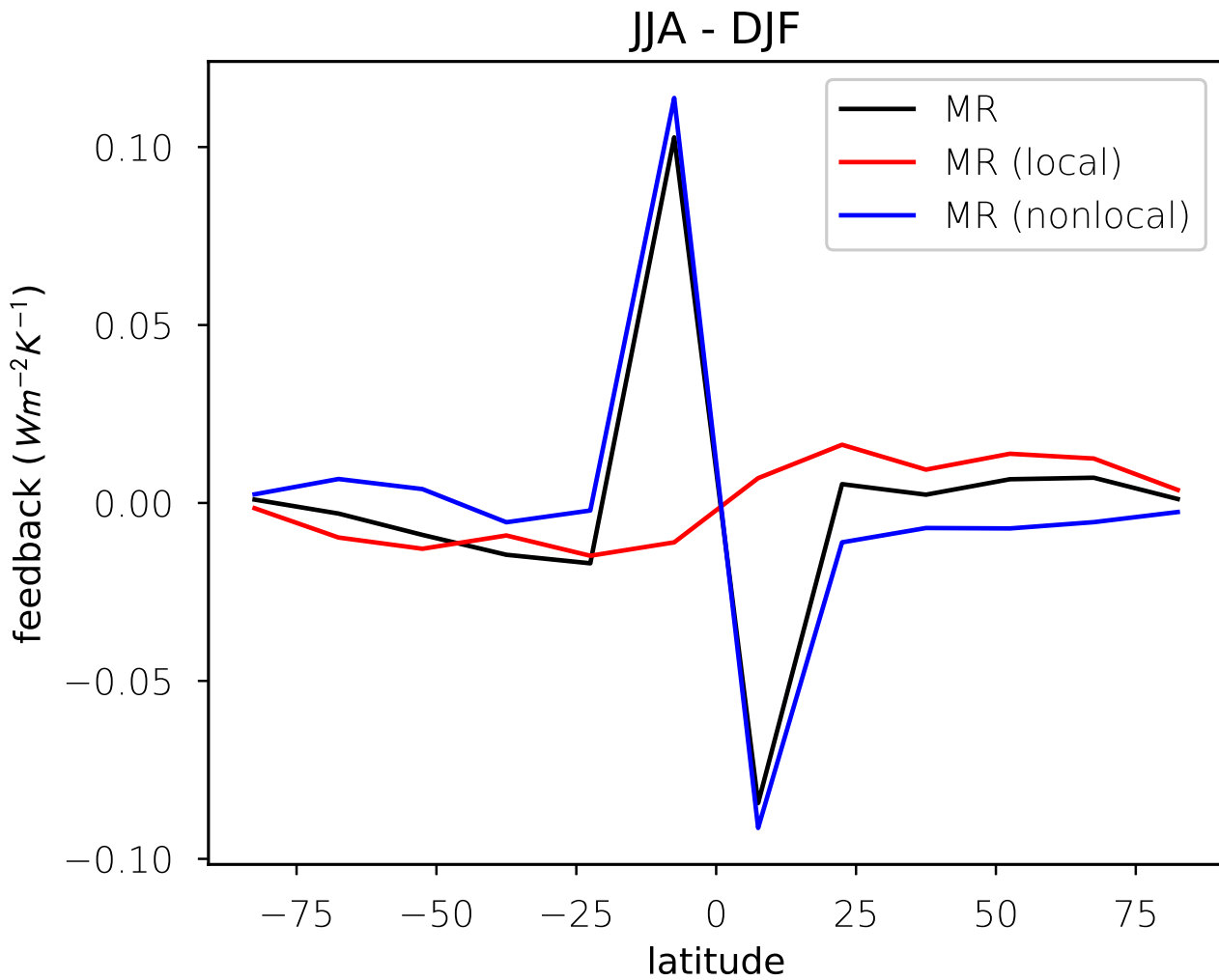
Figure S25: Difference between the multi-model zonal mean of the Jun/Jul/Aug and Dec/Jan/Feb net feedback. The pattern is largely determined by the nonlocal feedbacks, which we have elsewhere shown are dominated by negative feedbacks in regions of tropical convection. We would expect these regions to follow the ITCZ into the summer hemisphere, as is consistent with the results in this figure. Note that while the global values of the local and nonlocal feedbacks are anticorrelated across models (Table S8), this cancellation does not hold spatially or seasonally, suggesting this cancellation is more than a statistical artifact.

References

Cao, L., L. Duan, G. Bala, and K. Caldeira, 2016: Simulated long-term climate response to idealized solar geoengineering. *Geophysical Research Letters*, URL http://dx.doi.org/10.1002/2016GL068079.

Choi, Y.-S., H. Cho, C.-H. Ho, R. S. Lindzen, S. K. Park, and X. Yu, 2014: Influence of non-feedback variations of radiation on the determination of climate feedback. *Theoretical and Applied Climatology*, **115 (1)**, 355–364, doi:10.1007/s00704-013-0998-6, URL https://doi.org/10.1007/s00704-013-0998-6.

Dufresne, J.-L., and Coauthors, 2013: Climate change projections using the IPSL-CM5 Earth System Model: from CMIP3 to CMIP5. *Climate Dynamics*, **40 (9)**, 2123–2165, doi:10.1007/s00382-012-1636-1, URL https://doi.org/10.1007/s00382-012-1636-1.

Mauritsen, T., and Coauthors, 2019: Developments in the MPI-M Earth System Model version 1.2 (MPI-ESM1.2) and Its Response to Increasing CO2. *Journal of Advances in Modeling Earth Systems*, **11 (4)**, 998–1038, doi:10.1029/2018MS001400, URL https://agupubs.onlinelibrary.wiley.com/doi/abs/10.1029/2018MS001400.

Nazarenko, L., and Coauthors, 2015: Future climate change under RCP emission scenarios with GISS ModelE2. *Journal of Advances in Modeling Earth Systems*, **7 (1)**, 244–267, URL http://dx.doi.org/10.1002/2014MS000403.

Proistosescu, C., A. Donohoe, K. C. Armour, G. H. Roe, M. F. Stuecker, and C. M. Bitz, 2018: Radiative Feedbacks From Stochastic Variability in Surface Temperature and Radiative Imbalance. *Geophysical Research Letters*, **45 (10)**, 5082–5094, doi:10.1029/2018GL077678.

Rind, D., G. A. Schmidt, J. Jonas, R. Miller, L. Nazarenko, M. Kelley, and J. Romanski, 2018: Multicentury Instability of the Atlantic Meridional Circulation in Rapid Warming Simulations With GISS ModelE2. *Journal of Geophysical Research: Atmospheres*, **123 (12)**, 6331–6355, doi:10.1029/2017JD027149, URL https://agupubs.onlinelibrary.wiley.com/doi/abs/10.1029/2017JD027149, https://agupubs.onlinelibrary.wiley.com/doi/pdf/10.1029/2017JD027149.

Rugenstein, M., and Coauthors, 2019: LongRunMIP - motivation and design for a large collection of millennial-length AO-GCM simulations. *Bulletin of the American Meteorological Society*, doi:10.1175/BAMS-D-19-0068.1, URL https://journals.ametsoc.org/doi/abs/10.1175/BAMS-D-19-0068.1.

Rugenstein, M. A. A., J. Sedláček, and R. Knutti, 2016: Nonlinearities in patterns of long-term ocean warming. *Geophysical Research Letters*, **43 (7)**, 3380–3388, URL http://dx.doi.org/10.1002/2016GL068041.

Spencer, R. W., and W. D. Braswell, 2008: Potential Biases in Feedback Diagnosis from Observational Data: A Simple Model Demonstration. *Journal of Climate*, **21 (21)**, 5624–5628, doi:10.1175/2008JCLI2253.1, URL https://journals.ametsoc.org/doi/full/10.1175/2008JCLI2253.1.

Spencer, R. W., and W. D. Braswell, 2011: On the Misdiagnosis of Surface Temperature Feedbacks from Variations in Earth's Radiant Energy Balance. *Remote Sensing*, **3 (8)**, 1603–1613, doi:10.3390/rs3081603, URL https://www.mdpi.com/2072-4292/3/8/1603.

Trenberth, K. E., Y. Zhang, J. T. Fasullo, and S. Taguchi, 2015: Climate variability and relationships between top-of-atmosphere radiation and temperatures on Earth. *Journal of Geophysical Research: Atmospheres*, **120 (9)**, 3642–3659, doi:10.1002/2014JD022887.

Voldoire, A., and Coauthors, 2019: Evaluation of CMIP6 DECK Experiments With CNRM-CM6-1. *Journal of Advances in Modeling Earth Systems*, **11 (7)**, 2177–2213, doi:10.1029/2019MS001683, URL https://agupubs.onlinelibrary.wiley.com/doi/abs/10.1029/2019MS001683.